Journal of Research

of the National

Bureau of Standards

Exposure Standardization
of Iodine-125 Seeds Used for Brachytherapy

T. P. Loftus

National Bureau of Standards, Gaithersburg, MD 20899

A method for calibrating iodine-125 seeds in terms of exposure has been established. The standard free-air ionization chamber, used for measuring soft x rays, was chosen for the measurements. Arrays of four to six seeds were used to enhance the ionization-current-to-background-current ratio. Seeds from an array were measured individually in a re-entrant chamber. The quotient of the exposure rate for the array by the sum of the ionization currents in the re-entrant chamber is the calibration factor for the re-entrant chamber. Calibration factors were established for three types of iodine-125 seeds. The overall uncertainty for the seed exposure calibrations is less than 6%.

Key words: calibration; exposure rate; free-air chamber; iodine-125 seed; re-entrant chamber; standards.

Introduction

The radionuclide iodine-125, encapsulated in titanium seeds, is used for brachytherapy. Presently the seeds are characterized by stating a range for the activities of a group of seeds, with the stated activity computed from measurements made external to the seeds. In order to achieve traceability to NBS exposure standards, a manufacturer requested that NBS establish an iodine-125 calibration service for the seeds. Calibration data in terms of exposure for this radionuclide would then be consistent with calibrations for the radionuclides cobalt-60, cesium-137, and iridium-192. This procedure has also been requested by medical physicists and is in accord with recommendations of the National Council on Radiation Protection and Measurements [1].[1]

Source Descriptions

Three types of iodine-125 seeds were supplied for measurement. One type incorporates a gold marker which separates two resin spheres on which the radionuclide is adsorbed. The dimensions of the seed and of

---

About the Author: T. P. Loftus is a physicist in the Dosimetry Group of the NBS Radiation Physics Division.

---

[1]Figures in brackets indicate the literature references at the end of this paper.

the spheres are shown in figure 1. The spheres are free to move in the seed as much as 1.5 mm with the result that the distribution of radiation near the end welds can change considerably.

A second type of source, also shown in figure 1, is a seed with the same dimensions as the gold-marker type, but with the radionuclide adsorbed on a silver wire 3.0 mm in length. The movement of the wire in the seed is restricted to 0.5 mm.

The third type of source, with higher activity than in the other two types, is one in which the gold marker sphere is replaced by another iodine-125-coated resin ball.

Mobility of the active material in the seeds does not appear to be an important factor in the primary standardization of the seeds, where good geometry measurements are made with a standard free-air ionization chamber, but movement of the active material affects the reproducibility of measurements in 4π geometry, as in the re-entrant ionization chamber used as a laboratory standard.

Standard Free-Air Chamber:
Measurement Conditions and Corrections

The instrument most nearly suitable for exposure measurements of radiation from iodine-125 is the Ritz [2] free-air ionization chamber (FAC). This is the standard

chamber used for all NBS instrument calibrations for x rays in the 20-kV to 100-kV region. Important factors in the use of the FAC for the iodine-125 measurements are the defined air volume of the chamber (about 5.5 cm³) and the mean background current (about 1.6 fA). With these constraints, an iodine source of at least 400 MBq (12 mCi) would be required to provide measurement conditions of minimal acceptability, i.e., background corrections no greater than 10% of the readings and a source-to-chamber distance of no less than 0.25 m. The limit on improvement of the measurement conditions is governed by the available activity per seed and the physical size of the source relative to the FAC volume-defining aperture.

The important FAC dimensions, and corrections relevant to exposure measurements of iodine-125, are given in table 1. The photon-scattering and electron-loss corrections are those developed for measurements of 30-kV x rays filtered by 0.5 mm Al. There is no significant change in those corrections for x-ray energies down to 20 kV. The air attenuation correction given is based on

measurements using the iodine-125 radiation. The magnitude of the air attenuation correction is in general agreement with corrections for x rays in the same energy region but is greater than the value calculated using mass attenuation coefficients [3] weighted for the source spectrum. The linear attenuation coefficient for air at room conditions based on the measurements is 1.5×10^{-3} cm^{-1}. The calculated coefficient is 0.4×10^{-3} cm^{-1}. In all subsequent computations, the measured coefficient was chosen to correct for air attenuation in the FAC and

Table 1. FAC dimensions, and corrections for measurement of iodine-125 radiation.

Diaphragm area	0.7867 cm²
Collector plate length	7.0003 cm
Air attenuation length	12.7 cm
Corrections:	
Air attenuation	1.018
Photon scattering	0.995
Electron loss	1.000
Recombination	1.000

296

for attenuation between the sources and the defining plane of the FAC aperture.

Source Arrays and Positioning Device

The maximum activity per seed (about 1.3 GBq, 36 mCi) is provided by the no-marker type seed (see table 2). To reduce the importance of background currents on the FAC measurements, the seeds were measured in groups.

Seeds of the same type were mounted on transparent tape and supported on a frame inside a thick-walled aluminum cylinder. They were affixed to the tape in a uniform array and the frame was positioned in the aluminum cylinder such that the array was in line with two diametrically opposite holes in the cylinder wall. The frame can be rotated while the center of the array is maintained at the center of rotation. The source array when in a vertical position is seen by the FAC as a source with dimensions 4.5 mm high and $0.8n$ mm wide, where n is the number of sources in the array. The number of seeds of each type ranged from four to six. The diameter of the FAC aperture is 10 mm, so these array dimensions do not present source-chamber alignment problems.

Two series of the three types of sources were measured on separate occasions. Information regarding the various groups is provided in table 2.

Source Array Exposure Measurements

Although the source positioning device allows rotation of the source arrays, the main thrust of the FAC exposure measurements was to establish a mean exposure rate from an array of sources for the direction perpendicular to the plane of the array. This approach was taken since the eventual calibration of an individual seed will be given as a mean exposure rate at unit distance for the direction perpendicular to the long axis of the seed. To determine the mean exposure rate for a group of seeds, their positions and orientations were randomized on the transparent tape to make different arrays. The results of the first series of measurements for the gold-marker seeds are given in table 3.[2] The mean

Table 3. First series exposure rate measurements for gold-marker type seeds (μR m^2/s)

Array	FAC dist. (m)	Number of measurements[1]	Array means	Mean for arrays
1	0.50	4	2.281	
2	0.50	1	2.350	2.320
3	0.50	7	2.328	
3	0.25	5	2.350	
4	0.25	1	2.359	2.353
5	0.25	3	2.351	

[1]Each measurement consists of an independent series of current measurements taken at different times.

for the three arrays at 0.50 m differs from the mean for the three arrays at 0.25 m by 1.5%, but the standard deviation of the mean for the 0.50 m data is 0.9%. Since different arrays were used (with one exception) for measurements at the two distances, the mean value for the exposure rate, for this group of seeds, is taken as the mean of the measurements for all the arrays. The mean for the arrays of gold-marker type sources in the first series is 2.336 μR m^2/s on 1980 Dec 6.5. It is unimportant that array number 3 is included twice in computing the mean exposure rate.

All decay corrections for this work were computed using a half-life of 58.9 days for iodine-125. This half-life was determined when measurements of five seeds, taken 145 days apart and corrected using a half-life of 60.14 days (5), were all found to be inconsistent with earlier measurements. The average difference was 3.6%, with a standard deviation of the mean of 0.2%. The long-term stability for the measurement system used was shown, by 10 radium-226 check-source measurements, to have a standard deviation of the mean of 0.3%. Correcting the apparent activity and exposure data for decay, the exposure rate at unit distance per unit of apparent activity is 41.3 nR m^2/"mCi"s.

Table 2. Iodine-125 seeds used for exposure measurements.

Type	Number of seeds	Apparent activity[1] ("mCi")	Assay date
First series			
Gold-marker	4	60	1980/12/01
No marker	4	142	1982/09/06
Silver-wire	5	114	1981/06/01
Second series			
Gold-marker	6	84	1983/02/21
No marker	4	103	1983/03/07
Silver-wire	6	95.4	1983/02/21

[1]The apparent activity, as determined by the 3M Co., is a measure of the effective radiation output from the seeds and is independent of seed wall thickness or source self-absorption. The actual activity in the seed is greater than the apparent activity. The apparent activities are taken from the labels on the 3M lead acontainers. The 3M Co. has used the term "mCi Comp." for apparent activity.

[2]The Si unit of exposure is the coulomb per kilogram (C/kg). This unit is not in general use, and the quantity exposure will probably be replaced by the quantity air kerma, which has the unit gray (Gy). As a result, the special unit roentgen (R) is used for exposure in this paper.

297

Calibration of a Re-Entrant Chamber for Routine Individual Source Measurements

A spherical aluminum re-entrant ionization chamber [4] was chosen as the means for transferring the FAC exposure data, for the mean exposure rate from an array, to exposure data for individual seeds. The original brass tube in the chamber was replaced with an aluminum tube with walls 0.64 mm thick. The new tube has an inside diameter slightly greater than the length of a seed and has a flat bottom. When the seed is dropped into the tube, it will lie horizontally and be constrained to take a position near the center.

The calibration of the re-entrant chamber consists in determining the quotient of the FAC exposure data, for an array of seeds, by the sum of the ionization currents produced in the chamber by individual seeds. The result is a calibration factor for the chamber in terms of exposure at unit distance per unit charge.

The mean exposures measured by the FAC are representative of exposure data for random seed orientations in the arrays. It is therefore necessary to randomize the seeds in the re-entrant tube to determine a mean ionization current for each seed. The variability of the currents with seed position is shown in table 4. The stan-

Table 4. First series gold-marker type iodine-125 seed measurements in the re-entrant ionization chamber. Data corrected to STP and reference time 1981 June 1.5.

Source number	Mean current for random seed position (pA)	Number of seed positions	Standard deviation of the mean (%)
1	18.50	6	1.0
2	18.91	5	0.3
3	18.76	5	1.2
4	19.52	4	1.9

dard deviation of the mean for seed number 4 is a factor of 10 greater than the same statistic for measurements of an undisturbed seed.

The re-entrant chamber current measurements must be corrected for recombination. Tests show the correction factor is about 1.004 for currents of about 100 pA and unity for currents of about 0.8 pA. Interpolation for

currents of about 20 pA (table 4) indicates the recombination correction is 1.001.

With the exposure data and re-entrant chamber currents corrected to the same date, the re-entrant chamber calibration factor for the first series of gold-marker type seeds is 3.842 kR m^2/C.

Iodine-125 Spectrum and Exposure Calculations

It is of interest to test the consistency of the iodine-125 exposure measurements with exposure data determined from other physical quantities. Such a check can be accomplished by comparison of exposure measurements with exposure data calculated from measurements of the iodine-125 spectrum, after attenuation in the seed wall, and decay data.

Iodine-125 decays by electron capture, producing tellurium x-rays, in addition to 0.0667 gamma rays per transition. Recent nuclear-decay data [5] are given in table 5, where energy-absorption data [3] are also listed. The equation used to compute the exposure rate at unit distance from a point source of unit activity in vacuum, is as follows:

$$\Gamma_0 = \frac{\dot{X}L^2}{A} = \frac{1}{4\pi W/e} \sum_i (PE\ \mu_{en}/\rho)_i$$

where $\dot{X}$ is the exposure rate at a distance L from a point source in vacuum

A is the activity of the source

W/e is the mean energy expended per unit charge in air (33.7 J/C)

P is the fraction of the nuclear transitions giving rise to photons of the associated energy

E is the photon energy

μ_{en}/ρ is the mass energy-absorption coefficient for air for photons of the associated energy.

The exposure rate at unit distance per unit activity computed using the above equation and the data in table 5 is 42.2 nR m^2/mCi s (after conversion to special units). The weighted mean uncertainty, for the value of P in

Table 5. Nuclear-decay and energy-absorption data used to calculate Γ_0 for iodine-125.

Radionuclide	Radiation type	Energy E (keV)	Number per transition P	Energy-absorption coefficient μ_{en}/ρ (m^2/kg)	$E\ P\ \mu_{en}/\rho$ (keV m^2/kg)
Tellurium-125	x ray Kα_2	27.2	0.398	0.0212	0.230
Tellurium-125	x ray Kα_1	27.5	0.742	0.0204	0.416
Tellurium-125	x ray Kβ	31	0.258	0.0140	0.112
Iodine-125	γ ray	35.5	0.0667	0.0094	0.022

table 5, is 1.8%, while the uncertainty given for the μ_{en}/ρ data is 2% in this energy region. Obviously different values of Γ_0 will result if different data for P, E, and μ_{en}/ρ are used. A commonly used value is 40.3 nR m²/mCi s [6].

Silver-Wire and No-Marker Type Seeds

The measurement procedures established for the gold-marker seeds were also used for the silver-wire and no-marker type seeds. Six arrays were measured for each type. The exposure data for the silver-wire type seeds are shown in table 6. These data are calculated from measurements at 0.25 m from the arrays. Table 7 gives the re-entrant chamber current measurements for each of the five silver-wire type seeds. The mean currents listed are the result of three independent sets of measurements, with each set the result of measurements for many randomized seed positions. With a correction for recombination of 1.004, the sum of the source currents is 562.4 pA. Correcting for decay to a consistent date and dividing the FAC exposure data by the sum of the re-entrant chamber currents gives a calibration factor of 4.467 kR m²/C for the first series of silver-wire type seeds.

The quotient of the exposure data, by the apparent activity given in table 2 for the same date is 40.64 nR m²/"mCi"s.

Exposure data for the first series no-marker type seeds are given in table 8. Six arrays of the four seeds, in randomized positions on the tape, were measured. The re-entrant chamber data are given in table 9 where the currents are corrected for recombination (1.004). The sum of these currents is 1.364 nA, and the quotient of the exposure data and re-entrant chamber data is 3.716 kR m²/C.

With corrections for decay, the quotient of the exposure data by the apparent activity given in table 2 is 38.30 nR m²/"mCi"s.

Second Series, Au-Marker, Ag-Wire and No-Marker Iodine-125 Source Measurements

Completely independent sets of measurements for each of the three types of iodine-125 seeds were carried out to check the validity of the initial re-entrant chamber calibration factors. It was discovered that some scattered radiation from the cylindrical aluminum source container was being measured by the FAC and that a correction of 0.993 to the exposure data was required. At this time, the half-life of 58.9 days was introduced and recombination corrections for the re-entrant chamber were measured and used in the calculations. (All these improvements are incorporated in the data given for the first series of measurements.) For the second

Table 6. First series exposure-rate measurements of Ag-wire type seeds measured at 0.25 m from the FAC (μR m²/s)

Array number	Number of measurements	Mean for 1981 June 1.5	Mean for all arrays	Standard deviation of the mean (%)
1	12	4.639		
2	5	4.593		
3	2	4.699	4.633	0.8
4	2	4.560		
5	2	4.762		
6	14	4.543		

Table 8. First series exposure data for No-marker type seeds measured at 0.25 m from the FAC (μR m²/s).

Array number	Means for 1982 Sept. 12.5	Mean exposure rate (μR m²/s)	Standard deviation of the mean (%)
1	5.040		
2	5.059		
3	5.060	5.068	0.2
4	5.070		
5	5.092		
6	5.086		

Table 7. First series Ag-wire type iodine-125 seed measurements in the re-entrant ionization chamber. Data corrected to STP and reference time 1981 July 23.5.

Source number	Mean current (pA)	Standard deviation of the mean (%)
11	115.8	0.1
12	112.4	0.5
13	110.4	0.4
14	110.3	0.9
15	111.3	0.7

Table 9. First series No-marker type seed measurements in the re-entrant chamber. Data are corrected to STP and reference time 1982 Sept 12.5.

Source number	Mean current for seven measurements (pA)		Standard deviation of the mean (%)
1	338.8		0.2
2	316.5		0.3
3	338.4		0.4
4	369.9		0.3

299

series of measurements, a lead plate 3 mm thick, and with an aperture matching the aperture in the aluminum cylinder, was used to eliminate the effect of scattered radiation on the FAC exposure measurements.

The measurement procedures established in the first series were for arrays of sources exclusively. In the second series, by using improved equipment it was possible to perform FAC measurements for single seeds as well. The data show that the FAC array measurements are not larger than the sum of the data for the individual seeds in the array. The data for the gold-marker seeds are given in table 10. The mean exposure rate, for the group of seeds, used to compute the re-entrant chamber calibration factor is the mean for all the measurements, i.e., the sums of the individual source measurements are averaged with the group measurements since there appears to be no significant statistical difference.

The results of many re-entrant chamber measurements of the gold-marker seeds are given in table 11.

The re-entrant chamber calibration factor is the quotient of the mean of the exposure data from table 10 by the sum of the re-entrant chamber currents corrected for recombination, i.e., 3.872 kR m²/C.

The data for the second series of measurements using the silver-wire sources are given in tables 12 and 13. The calibration factor for the re-entrant chamber computed from these data is the quotient of the mean for all FAC measurements by the sum of the mean re-entrant chamber currents corrected for recombination, or 4.400 kR m²/C.

The data for the second series of measurements for the no-marker type sources are given in tables 14 and 15. There is almost 2% difference between the single source sum data and the array data for exposure measurements. Since no significant difference for the two types of measurements was observed for the gold-marker and silver-wire sources, the large difference is believed to be random, and all data are included in the average for the exposure rate at unit distance. The quotient of the mean for the exposure data by the sum of the re-entrant chamber currents for the sources, corrected for recombination, is 3.701 kR m²/C.

Table 10. Second series gold-marker type iodine-125 source exposure measurements at 0.25 m from the FAC (μR m²/s).

Type of measurement	Number of measurements	Mean exposure data 1983 Feb 1.5	Standard deviation of the mean (%)
Single source, sum.	4	4.047	0.9
Arrays	5	4.054	0.7

Table 11. Re-entrant chamber current measurements for second series gold-marker iodine-125 seeds.

Source number	Number of measurements	Mean current 1983 Feb 1.5 (pA)	Standard deviation of the mean (%)
1	17	170.8	0.7
2	15	167.4	0.5
3	16	181.9	0.4
4	16	179.5	0.3
5	16	175.7	0.4
6	16	166.4	0.5

Sum 10.42 nA

Table 12. Second series exposure measurements for silver-wire type iodine-125 sources at 0.25 m from the FAC (μR m²/s).

Type of measurement	Number of measurements	Mean exposure data 1983 Feb 1.5	Standard deviation of the mean (%)
Single source, sum.	5	5.613	1.3
arrays	8	5.688	1.0

Table 13. Re-entrant chamber current measurements for second series silver-wire sources.

Source number	Mean current 1983 Feb 1.5 (pA)	Number of measurements	Standard deviation of the mean (%)
1	208.6	6	0.2
2	219.5	6	0.5
3	195.0	6	0.2
4	228.9	7	0.7
5	230.4	11	0.8
6	198.7	6	0.9

Table 14. Second series exposure measurements for No-marker type iodine-125 sources at 0.25 m from the FAC (μR m²/s).

Type of measurement	Number of measurments	Mean exposure data 1983 Feb 1.5	Standard deviation of the mean (%)
Single source, sum.	3	5.490	0.3
Arrays	9	5.595	0.3

Table 15. Second series re-entrant chamber current measurements for the No-marker type sources.

Source number	Mean current[1] 1983 Feb 1.5 (pA)	Standard deviation of the mean (%)
1	367.4	0.2
2	388.4	0.2
3	361.8	0.2
4	381.1	0.3

[1]Currents for nine random source positions in re-entrant tube.

Summary of Calibration Factor Data for Re-Entrant Chamber

The calibration factors for the re-entrant chamber are summarized in table 16. The mean difference between the two independent sets of determinations of the calibration factors, referenced to their means, is 0.9%

Comparison of Iodine-125 Source Calibrations: Exposure and Activity

A direct comparison of the exposure measurements and exposure data calculated from spectral measurements was made possible through the cooperation of the NBS Radioactivity Group. Two sources, one a gold-marker type and one a silver-wire type, were calibrated after decaying to activities within the range of radioactivity measurement equipment. The data are provided in tables 17 and 18 where n is the number of photons per unit time. The two sources were then calibrated for exposure using the re-entrant chamber and the calibration factors appropriate to their types. A comparison of the results is shown in table 19. It should be noted that although little self-scattered radiation was observed in the radioactivity measurement it is not counted, whereas the FAC with no discrimination will measure self-scattered radiation.

A problem associated with the use of activity as a measure for iodine-125 seeds is illustrated by the different values for this quantity which can be calculated from the spectrum for the gold-marker source (table 17) and decay data (table 5). Using $A = n/P$ and the data for the 35.5-keV gamma ray, the computed activity is 2.5 MBq (69 μCi). If the data for the Te Kβ 31-keV x ray are

used, the activity is 2.9 MBq (78 μCi); if the Te Kα data are used, the activity is 2.7 MBq (72 μCi). As a result, calculated gamma-ray exposure constants will differ depending on the reference radiation.

Directional Dependence of Radiation from Iodine-125 Source Arrays

The calibration procedure for the iodine-125 seeds is designed to provide data for radiation emitted perpendicular to the seed axis. Since the seeds are implanted in tissue, the variation of exposure with direction from the source is of interest. Measurement of this characteristic was carried out by rotating the source arrays through 180° by means of the device already described. The exposure rate from a source array was found to be nearly a linear function of the sine of the azimuthal angle of the array (at 0 degrees, the source axes are parallel to the axis of the FAC). Normalized exposure data and $\dot{X}_n = f(\sin \theta)$ are shown in figures 2 and 3. The data were normalized to unity at $\theta = \pi/2$. The constants for the equations result from a least-squares fit to the data of a first order polynomial in $\sin \theta$. A mean exposure rate from a seed can be computed by averaging $f(\sin \theta)$ over all solid angles so that

$$\bar{\dot{X}}_n = \frac{\int_0^\pi \dot{X}_n \sin \theta \, d\theta}{\int_0^\pi \sin \theta \, d\theta} = a + \frac{\pi b}{4}.$$

Table 16. Re-entrant chamber calibration factors (kR m²/C).

Source type	First series	Second series	Mean calibration factor
Gold-marker	3.842	3.872	3.857
Silver-wire	4.467	4.400	4.433
No-marker	3.716	3.701	3.708

Table 17. Measurements of gold-marker iodine-125 source spectrum (1983 Feb 21.44) and energy-absorption data.

Radiation type	E (keV)	n (s⁻¹)	μ_{en}/ρ (m²/kg)	$nE \, \mu_{en}/\rho$ (keV m²/kg)
Te Kα	27.4	2.402×10⁶	0.0210	1.382×10⁶
Te Kβ	31	5.867×10⁵	0.0140	2.546×10⁵
γ	35.5	1.340×10⁵	0.00935	4.448×10⁴

Table 18. Measurements of silver-wire iodine-125 source spectrum (1983 Feb 20.45) and energy-absorption data.

Radiation type	E (keV)	n (s⁻¹)	μ_{en}/ρ (m²/kg)	$nE \, \mu_{en}/\rho$ (keV m²/kg)
Te Kα	27.4	2.836×10⁶	0.0210	1632×10⁶
Te Kβ	31	7.028×10⁵	0.0140	3.050×10⁵
γ	35.5	1.962×10⁵	0.00935	6.512×10⁴
Ag Kα	22.1	6.59 ×10⁵	0.0400	5.826×10⁵
Ag Kβ	25.2	1.61 ×10⁵	0.0268	1.087×10⁵

Table 19. Comparison of exposure calibration data, $\dot{X}$(FAC) and exposure data computed from measurements of spectrum, $\dot{X}(A)$.

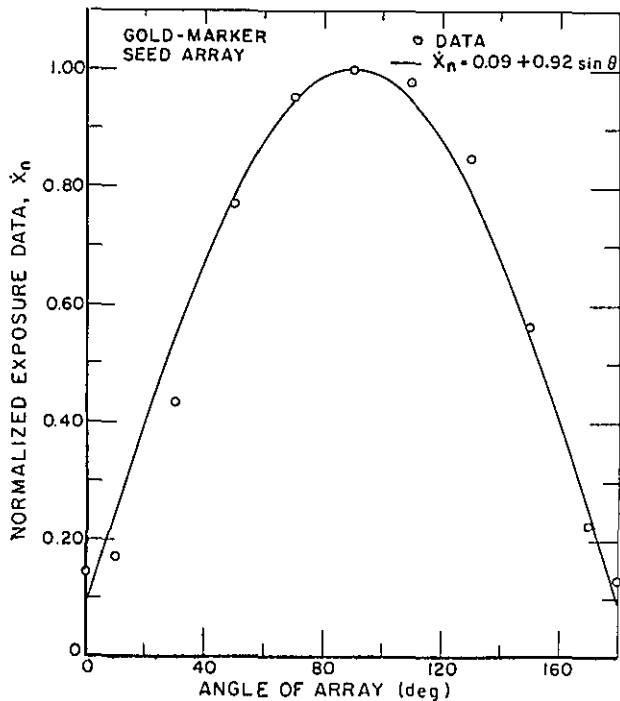| Source type	Exposure calibration (nR m²/s)	Exposure from spectrum (nR m²/s)	Ratio $\dot{X}$(FAC)/$\dot{X}$(A)
Gold-marker	3.271	3.117	1.049
Silver-wire	5.138	4.936	1.041

301

Figure 2—Standard free-air ionization chamber measurements of exposure rate from an array of gold-marker type iodine-125 seeds. The array was rotated through 180° starting and ending with the ends of the seeds facing the FAC diaphragm. The data are normalized to measurements with the plane of the array perpendicular to the FAC axis.

The values for the constants and for $\bar{X}_n$ are given in table 20. Higher order polynomials provide equations which fit the data better but the mean value for $\dot{X}_n$ does not change when they are used. The mean exposure rates given in table 20 are for normalized data and are fractions of the exposure rates perpendicular to the long axis of the seeds. The results are in general agreement with the results of other authors [7,8].

Table 20. Constants for the relation $\dot{X}_n = a + b \sin \theta$, and the normalized mean exposure rates for two seed types. The mean exposure rate is derived from data which were normalized to the exposure rate from the array in a direction perpendicular to the plane of the array.

Source array	a	b	$\bar{X}_n$
Silver-wire	0.20	0.85	0.87
Gold-marker	0.09	0.92	0.81

Uncertainties for Iodine-125 Exposure Standardization

The uncertainty for an exposure-rate calibration of an iodine-125 seed is dependent on the seed type. For each type, all random uncertainties, represented by standard
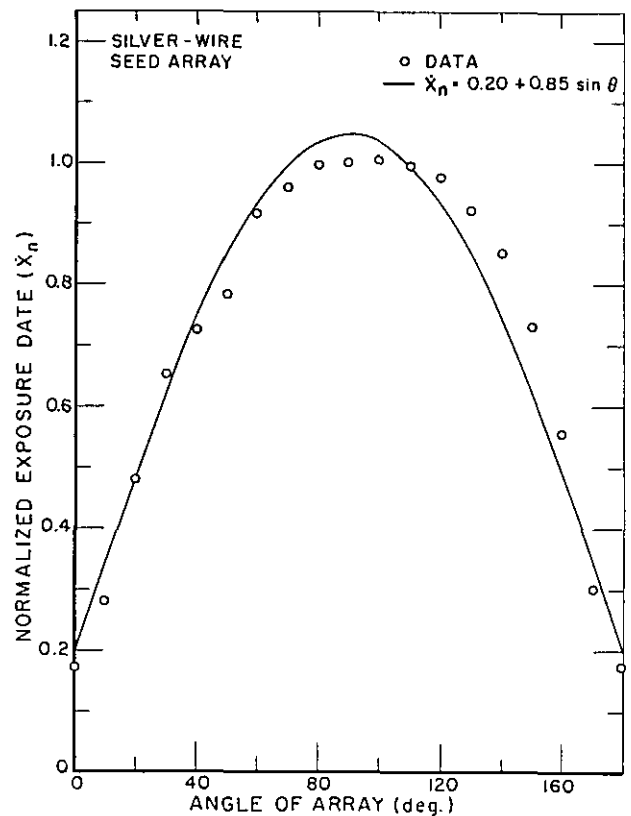

Figure 3—Standard free-air ionization chamber measurements of exposure rate from an array of silver-wire type iodine-125 seeds. The array was rotated through 180° starting and ending with the ends of the seeds facing the FAC diaphragm. The data are normalized to measurements with the plane of the array perpendicular to the FAC axis.

deviations, and all remaining estimated uncertainties, which are treated like standard deviations, are added in quadrature to provide an estimate of the combined uncertainty. The random uncertainties in the determination of the re-entrant chamber calibration factor are the standard deviation of the mean for the exposure rate measurements of the group of sources, and the standard deviation of the mean for the total current in the re-entrant chamber. These are given in table 21 for the first and second series of measurements. In this table, n is the number of sources in the array. The percentage given is the square root of the sums of the squares of the percent standard deviations of the means for each source. The standard deviation of the mean for each source is calculated from source measurements for random positions in the re-entrant tube.

The estimated uncertainties for the standard free-air chamber and re-entrant chamber are 1.2% [2] and 0.2%, respectively. The random uncertainties and the estimated uncertainties are added in quadrature to form a combined uncertainty. To the combined uncertainty for

302

Table 21. Summary of standard deviations of the mean, σ_m, for exposure and re-entrant chamber current summations.

Source type	First series				Second series			
	No. of arrays	σ_m FAC (%)	n	σ_m re-ent. (%)	No. of arrays	σ_m FAC (%)	n	σ_m re-ent. (%)
Gold-marker	5	0.6	4	2.5	9	0.5	6	1.8
Silver-wire	6	0.8	5	1.3	13	0.8	6	1.5
No-marker	6	0.2	4	0.6	12	0.3	4	0.2

the re-entrant chamber calibration factor must be added the random uncertainty for the mean of several measurements of a seed in the re-entrant chamber during a calibration. This is estimated to be 0.4%.

The combined uncertainty is multiplied by 2 to give an overall uncertainty that corresponds roughly to a 95% confidence interval. The combined and overall uncertainties are given in table 22.

Table 22. Combined and overall uncertainties for iodine-125 seed calibrations. The first and second series uncertainties are averaged to form the combined uncertainties.

Seed type	Combined (%)	Overall (%)
Gold-marker	2.6	5
Silver-wire	2.1	4
No-marker	1.5	3

The author wishes to acknowledge the many helpful suggestions of Dr. Robert Loevinger in editing this report.

References

[1] National Council on Radiation Protection and Measurements Report No. 41, 23 pages; April 1974. Specification of gamma-ray brachytherapy sources. NCRP Publications, 7910 Woodmont Ave., Suite 1016, Washington, DC 20014.

[2] Ritz, V. H. Standard free-air chamber for the measurement of low energy x rays (20 to 100 kilovolts-constant-potential). J. Res. Natl. Bur. Stand. (U.S.). **64C**: 49-53; 1960.

[3] Hubbel, J. H. Photon mass attenuation and mass energy-absorption coefficients from 1 keV to 20 MeV. Int. J. Appl. Radiat. Isot. **33**: 1269-1290; 1982.

[4] Loftus, T. P. Standardization of iridium-192 gamma-ray sources in terms of exposure. J. Res. Natl. Bur. Stand. (U.S.). **85**: 19-25; (1980).

[5] National Council on Radiation Protection and Measurements Report No. 58, 506; 1978. A handbook of radioactivity measurements procedures. NCRP Publications, 7910 Woodmont Ave., Suite 1016, Washington, DC 20014.

[6] Krishnaswamy, V. Dose distribution around an iodine-125 seed source in tissue. Radiology **126**: 489-491; 1978.

[7] Sondhaus, C. A. Modern interstitial and intracavitary radiation management. New York: MASSON Publishing, Inc., 1981. Chap. 9, pp. 83-101.

[8] Ling, C. C., et al. Physical dosimetry of ^{125}I seeds of a new design for interstitial implant. Int. J. Radiat. Oncol. Biol. & Phys. In press.

Stability of Small Industrial
Platinum Resistance Thermometers

B. W. Mangum

National Bureau of Standards, Gaithersburg, MD 20899

This paper reports the results of an investigation of the stability of a selection of small industrial platinum resistance thermometers (IPRTs) upon heat treatment and handling. Ninety-four IPRTs, of several models, obtained from five manufacturers were studied. Most of the IPRTs exhibited calibration drifts and also effects due to the presence of moisture or strain. There was no apparent improvement in the stability if the resistance ratio, $R(t)/R_0 = W(t)$, instead of resistance were used as the criterion. Comparisons are made of the relative stability of the products of the five companies.

Key words: Industrial platinum resistance thermometers (IPRTs); platinum resistance thermometers (PRTs); temperature; thermometers; thermometry.

Introduction

Industrial platinum resistance thermometers (IPRTs) are usually considered to have several advantages over other types of thermometers. The IPRTs have a fairly low resistance (about 25 Ω to 2000 Ω), are usable over a wide temperature range and to high temperatures, are available in a variety of sizes and shapes, are said to be fairly rugged, and have a nearly linear resistance-versus-temperature relationship. Some of their disadvantages are that they have a temperature sensitivity of only 0.4% change in resistance per kelvin and that they may have limited stability.

The use of IPRTs in industry, in monitoring the operation of electric generating plants, and by instrument manufacturers has been increasing over the past several years and is now widespread. Despite this, prior to 1982 there was very little information in the literature about their performance [1-5][1] and especially in the very important region from about 0 °C to 250 °C. In 1982, several papers on IPRTs were presented at the Sixth

---

About the Author: B. W. Mangum is a physicist in NBS' Temperature and Pressure Division.

---

[1]Figures in brackets indicate literature references at the end of this paper.

International Symposium on Temperature [6-11]. In a preliminary report [11] at that Symposium, we presented results of an investigation of the stability of 60 IPRTs upon thermal cycling and normal handling.

It should be clear that IPRTs are not intended to be replacements or substitutes for Standard Platinum Resistance Thermometers (SPRTs) [12]. The SPRT is intended to be used in the laboratory where accuracy and stability are of foremost importance, whereas the IPRTs are intended for industrial applications where generally a compromise must be made among several important features which include not only accuracy and stability, but also interchangeability, size, ruggedness, response time, and cost. Because of the method of fabrication, IPRTs have several features that are either nonexistent or negligible in SPRTs. The platinum wire of IPRTs is fully supported [9] in order to protect the thermometer from mechanical shock and this may lead to contamination, a problem not encountered with SPRTs. Also, there is a problem of strain in IPRTs caused by the difference in the thermal expansion of the platinum and the material on which it is mounted [9]. This problem is absent or causes errors that are negligible in SPRTs.

This article reports results of the investigation of 94 IPRTs, including those of the 60 IPRTs reported at the Sixth International Symposium on Temperature [11]. Products of five IPRT manufacturers were included in

this study[2]. The stability of those IPRTs was evaluated over the range from 0 °C to 100 °C after being heat-treated for some time at a temperature near 250 °C.

Experimental Details

Selection of IPRTs

The thermometers that we investigated were obtained from the five manufacturers listed in table 1. The IPRTs obtained for the study were representative of the usual industrial productions of these companies. Although there are other manufacturers of IPRTs, it was thought that the products of these five companies are representative of all commercially available IPRTs. A

Table 1. Manufacturers whose products were investigated in this study.

Burns Engineering, Inc.
Engelhard Industries
Minco Products, Inc.
Rosemount, Inc.
H. E. Sostman & Co. (now Sostman Division of Yellow Springs Instruments, Inc.)

total of 94 IPRTs comprising 35 models from these companies was investigated. Table 2 contains a list of the manufacturers (by their code letters), the number of different models or styles represented by the products from each manufacturer, the number of IPRTs of each model or style from each manufacturer, and the total number of IPRTs from each manufacturer. As indicated in table 2, our study did not include the same number of

Table 2. Industrial platinum resistance thermometers investigated.

Manufacturer	Number of models represented	Number of IPRTs of each model	Total number of IPRTs from each manufacturer
A	19	1, 3, 3, 4, 3, 1, 3, 2, 3, 1, 1, 1, 2, 5, 1, 3, 2, 2, 2	43
B	6	6, 4, 4, 3, 1, 1	19
C	4	2, 1, 1, 3	7
D	6	2, 5, 2, 1, 2, 2	14
E	6	2, 3, 2, 1, 2, 1	11

[2]Certain commercial equipment, instruments, or materials are identified in this paper in order to adequately specify the experimental procedure. Such identification does not imply recommendation or endorsement by the National Bureau of Standards, nor does it imply that the materials or equipment identified are necessarily the best available for the purpose.

IPRTs from each of the companies. The nominal resistances of the IPRTs at 0 °C, i.e., their R_0 values, ranged from 50 ohms to 2000 ohms and the distribution of the different R_0 values is given in table 3. With the exception of 8 IPRTs, the maximum operating temperature as specified by the manufacturers was in the range 250 °C to 1000 °C.

Table 3. Ice-point resistance distribution of IPRTS.

R_0 (Ω)	Number of IPRTs
50	2
100	63
200	7
425	2
470	4
500	2
550	3
1000	3
1250	1
2000	7

Thirteen IPRTs were fairly large in that their sheaths were about 0.25 inches in diameter and varied in length from 2.5 to 14 inches.[3] Four of these had tapered sheaths so that the diameter of the sheaths in the sensitive region of the IPRT was 1/8 inch. Another 14 IPRTs had sheaths with diameters of 1/8 inch and lengths of 5.5 inches. Four surface sensor types were quite large also; the dimensions of one of these were 0.75×0.50×0.10 inches and of the other three were 1.00×0.75×0.10 inches. The remaining 63 IPRTs were much smaller in size, usually of the order of 1/8 inch in diameter and perhaps 1/2 to 1 inch long for the probe-type sensors and perhaps 1/8×1/8×0.05 inches for the surface sensor type. Some of the IPRTs had two leads, some had three leads, and others had four leads. In all cases, four lead-wires from the measuring equipment were either welded to or soldered with Au-Sn eutectic solder to the leads of the IPRTs, as close to the thermometers as practicable if four sufficiently long lead-wires were not provided on the IPRTs by the manufacturer.

The temperature-sensitive elements of all the IPRTs were constructed of platinum wire. Although IPRTs comprised of platinum films are available commercially, the stability of that type of sensor was not investigated because of their greater tendency toward hysteresis. The methods of construction, the methods of supporting the platinum wire elements, the encapsulation of the platinum elements and their supports, and the physical dimensions of the IPRTs varied from manufacturer to

[3]Since the dimensions help identify the size of the units, and are in common usage, we have not used the SI unit (i.e., cm).

manufacturer and from model to model of a given manufacturer. The surface temperature sensors had encapsulations of ceramic, stainless steel, or platinum. The probe-type IPRTs contained the platinum elements in glass, ceramic, stainless steel, gold-plated brass, or gold-plated Kovar.

Equipment

An ice bath provided the temperature for the calibration of the IPRTs at 0 °C. A well-stirred, temperature-controlled oil bath provided the other temperatures in the range from 0 °C to 100 °C at which the IPRTs were tested. The temperature controller used a thermistor as the temperature sensing element. In the range from 20 °C to 60 °C, the temperature of the oil bath was regulated to $\leqslant \pm 1$ mK, whereas in the range from about 80 °C to 100 °C, the nonuniformity and fluctations in the bath increased to $\leqslant \pm 2$ mK. The oil bath temperatures were measured with an SPRT. The triple point of water was the reference point for the SPRT. The resistances of the SPRT and the IPRTs were measured with an automatic ac bridge [13] operating at 384 Hz and having a resolution of 1 part in 10^7. The bridge provided a constant current for the SPRT and a constant power for the IPRT measurements. The IPRTs were connected via a scanner to a microcomputer that controlled their calibration measurements and also their switching by the scanner.

A three-zone furnace was used to heat-treat the IPRTs at 235 °C. The temperature of the furnace was controlled at the set point to within ± 2 °C.

Measurement Procedure

Ten sets of 10 IPRTs each were comprised of the 94 IPRTs investigated. Set X contained five IPRTs that had been studied previously in set VI, and set IX contained one IPRT that had been studied previously in set III. Except for the six IPRTs of sets IX and X that had been studied during the investigation of sets III and VI, the IPRTs for each set were selected arbitrarily from the products of the five manufacturers. There was no statistical selection of the thermometers. Two sets of IPRTs were studied concurrently.

The measurement protocol used in investigating the stability of the IPRTs upon thermal treatment and handling was as follows. The tests began by calibrating the IPRTs of a given set at 0 °C, 20 °C, 40 °C, 60 °C, 80 °C, and 100 °C. Measurements were made with the IPRTs located directly in the oil of the temperature-controlled oil bath or in a tube of oil immersed in an ice bath. The power dissipated in the IPRTs during measurements was 20 μW and, as we will see later, the self-heating was negligible (i.e., equivalent to <1 mK). Furthermore, the IPRTs were sufficiently immersed (12 to 15 cm) in the

bath fluid that the effects of the external environment were negligible.

Following calibration at the six temperatures, the IPRTs were placed in a glass tube in a cold furnace. The system, which was constructed so that it could be purged, was flushed with argon for 15 minutes and then the furnace heated to 235 °C, while continuing to pass argon through the system. After 15 minutes, the furnace would be at the desired temperature of 235 °C. The IPRTs were left in the furnace at that temperature for an additional 24 hours, with argon continuing to flow slowly through the system. At the end of the 24-hour heat-treatment period, the furnace was turned off. Thirty minutes later, the flow of argon was stopped and the IPRTs removed. Then, usually over the next two days, the resistances of the sensors were measured again at the same six temperatures at which they were calibrated previously. With the exception of sets I and II, the heat treatment and measurement cycle as just described was repeated nine times, for a total of 10 heat treatment periods followed by calibration.

For sets I and II, on which the measurements were started first and with which the measurement design was developed for the remaining sets, the situation was somewhat different. The lead-wires of the IPRTs of those sets had been initially soldered to the lead-wires going to the scanner with Pb, anticipating no problems since the IPRTs were to be heated always in an argon atmosphere. Unfortunately, during the heat-treatment of the IPRTs, oxidation of the solder junctions occurred slowly, presumably due to air in the oil remaining in the Teflon tubing around the junctions. This became apparent during the measurements by the erratic behavior of the resistances of the IPRTs. After the 15th thermal cycle, the Pb-soldered junctions of set I were replaced with welded junctions and those of set II were replaced with soldered junctions using Au-Sn eutectic solder. In subsequent tests, no deterioration of these new junctions and no differences in the behavior of the welded and the Au-Sn eutectic soldered junctions were observed. Based on the performance of these new junctions, the remaining IPRTs were connected to the measurement system lead-wires by means of Au-Sn eutectic solder, which was a simpler operation than welding.

Experiments were performed during the early thermal cycles of sets I and II to determine the appropriate conditioning time for the IPRTs at 235 °C. Based on the results of heat-treatment times of 2 hours, 6 hours, 24 hours, and 30 hours, a heating time of 24 hours was selected. There were no apparent differences among the results for 6 hour, 24 hour, and 30 hour heat-treatment times, so a 24 hour heating time was selected as being a reasonable compromise.

Discussion of Errors

Errors in Resistance Measurements

Resistance measurements of the SPRT for temperature determinations and of the IPRTs at the various test temperatures were made with an automatic ac bridge [13], a simplified version of which has been described by Brown, et al. [14]. The uncertainty of any one measurement with this bridge was estimated to be ± 4 parts in 10^7. An average of 10 resistance measurements, rather than an individual measurement, was taken as the resistance value of the SPRT or of an IPRT at a given temperature. By this technique, the uncertainty in the resistance measurements could be reduced to an estimated ± 2 parts in 10^7.

Errors in Temperature Measurements

The SPRT used in temperature measurements had been previously calibrated by the Platinum Resistance Thermometer Calibration Laboratory of the National Bureau of Standards [12]. That calibration consisted of resistance measurements of the SPRT at the triple point of water and the freezing points of tin and zinc. The uncertainties in realizing those fixed points of the International Practical Temperature Scale of 1968 (amended addition of 1975) [15] (IPTS-68) are ± 0.1 mK for the triple point of water and ± 1 mK for the freezing points of tin and zinc. The combination of these yields an uncertainty in the calibration of ± 0.4 mK. This is important in the accurate determination of temperatures but is immaterial in our investigation of the stability of IPRTs since the sensors were tested always at the same temperatures.

The estimated uncertainties in the ac bridge measurements correspond to an uncertainty in temperature of about ± 0.1 mK.

The fluctuations in the bath fluid temperature were larger at 80 °C and 100 °C than at the lower temperatures because of the reduced sensitivity at the higher temperatures of the thermistor used as the control sensor of the temperature controller. The magnitude of the uncertainty at 80 °C and 100 °C was estimated to be $\leqslant \pm 2$ mK. At lower temperatures, the uncertainty in the measured temperature was estimated to be $\leqslant \pm 1$ mK.

The uncertainty in the temperature of the conditioning furnace was estimated to be ± 2 °C. It is thought that this uncertainty did not play a significant role in the behavior of the IPRTs.

Errors Due to Self-Heating

An experiment was performed to ascertain the amount of self-heating of the IPRTs when their re-

sistances were being measured with 10 μW and 20 μW of power being dissipated. The results indicated that the maximum amount of self-heating at 20 μW was $\leqslant 1$ mK. The uncertainty in the resistance measurements due to changes in the self-heating was much less than the equivalent of 1 mK, however, and that is the relevant uncertainty since our primary interest was in *changes* of IPRT resistance. During stability measurements, the resistances were measured always with 20 μW of power being dissipated in the IPRTs.

Errors Due to Inadequate Immersion

For all resistance measurements in the temperature range 0 °C to 100 °C, the IPRTs were immersed 12 to 15 cm in either the well-stirred constant-temperature-bath oil or in the oil in the thermometer well of the ice bath. The adequacy of immersion was checked and it was found that the uncertainty in the measurements due to improper immersion was negligible. The uncertainty was within that of the resistance measurements.

Results and Analysis

Two of the 94 IPRTs investigated failed (open circuit) during the course of the heat treatments, one of them functioning normally through six heat treatments before failing. Essentially three types of behavior were exhibited by the IPRTs that maintained their integrity throughout the series of thermal treatments. Of the 92 IPRTs that did not fail during the tests, 39 underwent decreasing resistances by amounts equivalent to from 2 mK to 900 mK. This type of behavior is exemplified by the results of IPRT RA3/9 shown in figure 1. Four of these 39 IPRTs had changes in resistance in excess of the equivalent of 200 mK over the course of the study. Thirty-four of the 92 IPRTs exhibited resistance increases by amounts equivalent to from 1 mK to 120 mK over the time of the 10 heat treatments and calibrations. This type of behavior of the IPRTs is exemplified by the results of IPRT PB9/55 shown in figure 2. An additional IPRT having this type of behavior had a very large change, in excess of the equivalent of 1 K. The remaining 19 IPRTs showed the third type of behavior, that of scatter in the results but no discernible drift. The behavior of these IPRTs is exemplified by the results of IPRT RE6/66 shown in figure 3.

One IPRT, PC2/40, that was tested as part of set III and five IPRTs, PA10/25, PA2/22, PD2002/21, PA1001/48, and RD4/11, that were tested as part of set VI were subsequently tested again as parts of sets IX and X, respectively. The results obtained for those sensors at 40 °C are shown in figure 4. Three of them developed discontinuities in their resistance temperature relationships by being kept at room temperature from the
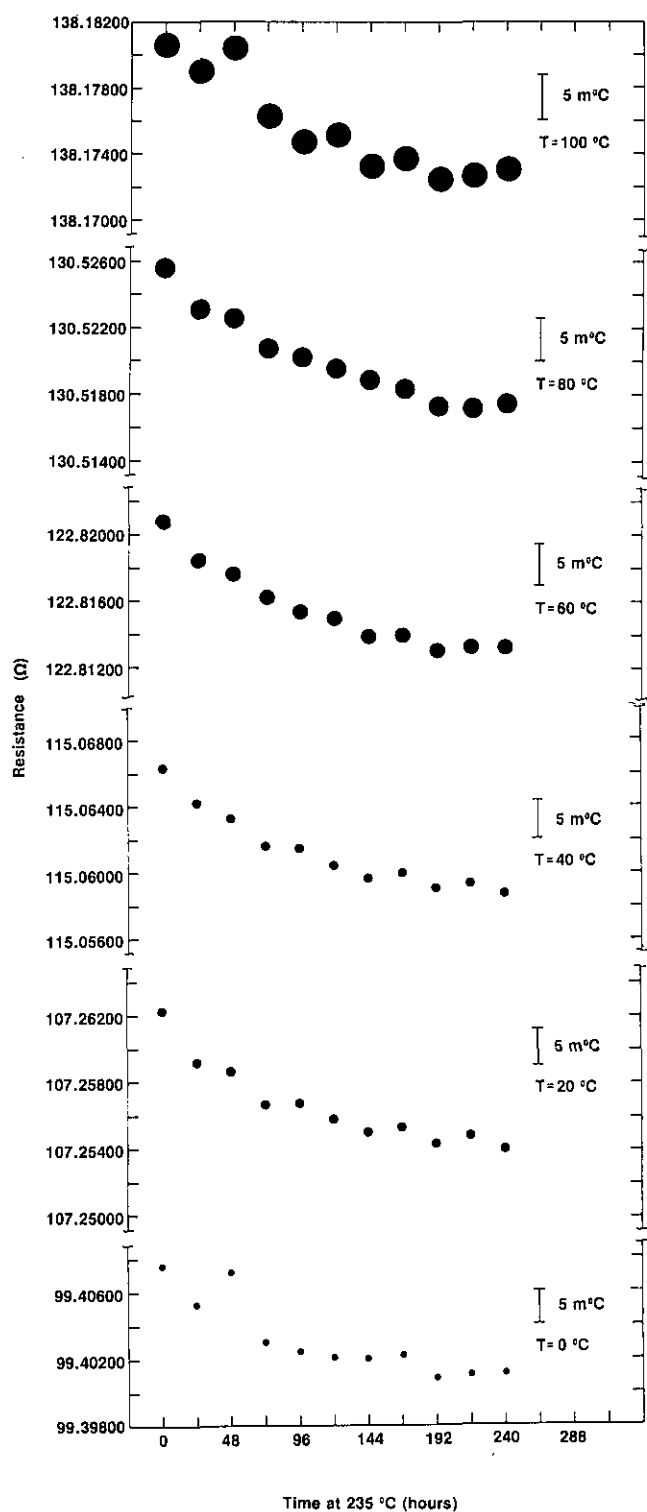
Figure 1—Variation of the resistance of IPRT RA3/9 with heat treatment. Measurements were made at 0 °C, 20 °C, 40 °C, 60 °C, 80 °C, and 100 °C, as indicated on the graph. Resistance differences expressed as equivalent temperature differences in m°C are indicated. Time 0 refers to the original calibration prior to heat treatment.
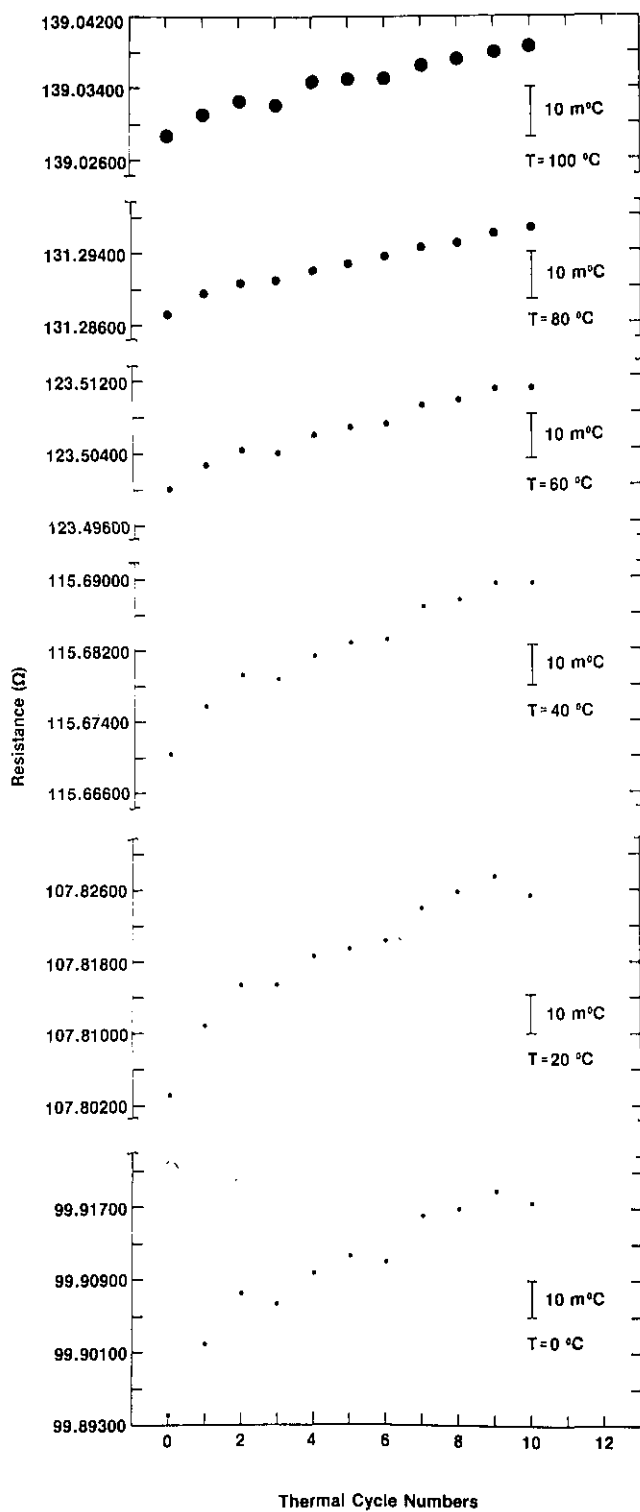
Figure 2—Variation of the resistance of IPRT PB9/55 with heat treatment. Measurements were made at 0 °C, 20 °C, 40 °C, 60 °C, 80 °C, and 100 °C, as indicated on the graph. Resistance differences expressed as equivalent temperature differences in m°C are indicated. Time 0 refers to the original calibration prior to heat treatment.

309

Figure 3—(Left)Variation of the resistance of IPRT RE6/66 with heat treatment. Measurements were made at 0 °C, 20 °C, 40 °C, 60 °C, 80 °C, and 100 °C, as indicated on the graph. Resistance differences expressed as equivalent temperature differences in m°C are indicated. Time 0 refers to the original calibration prior to heat treatment.
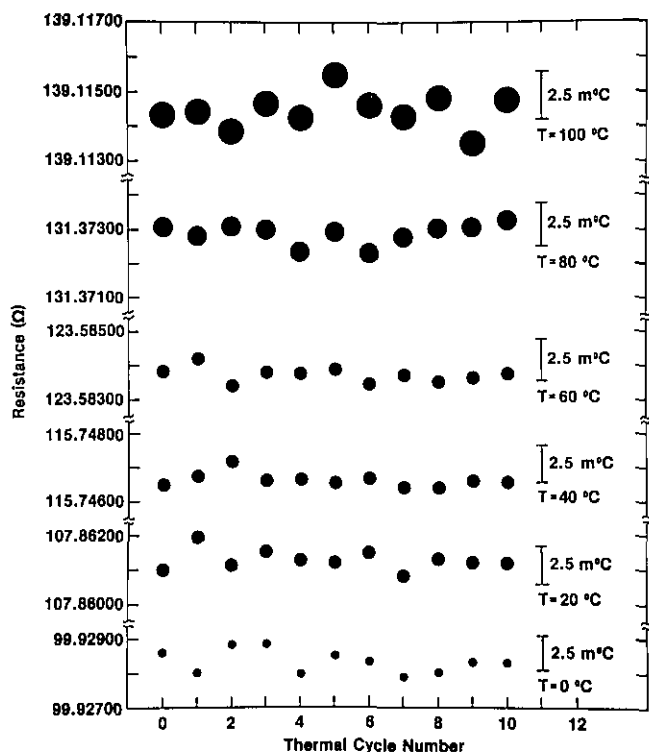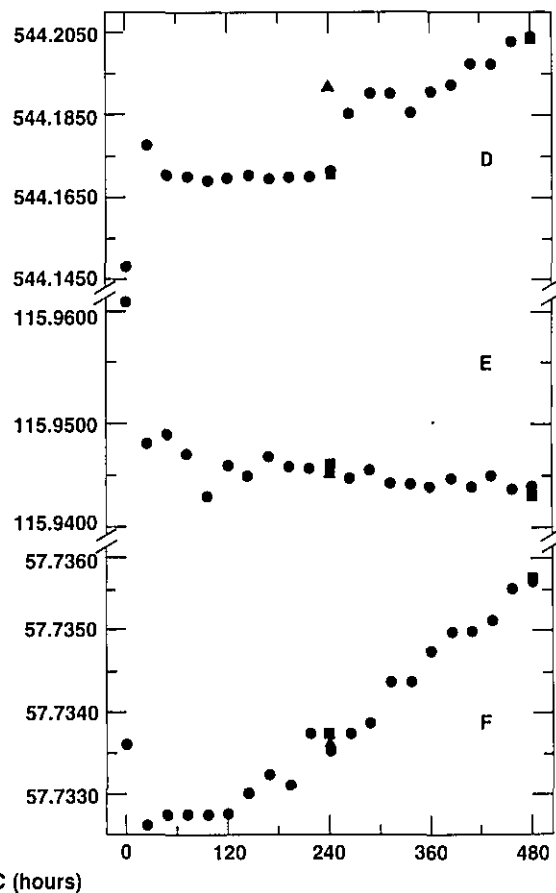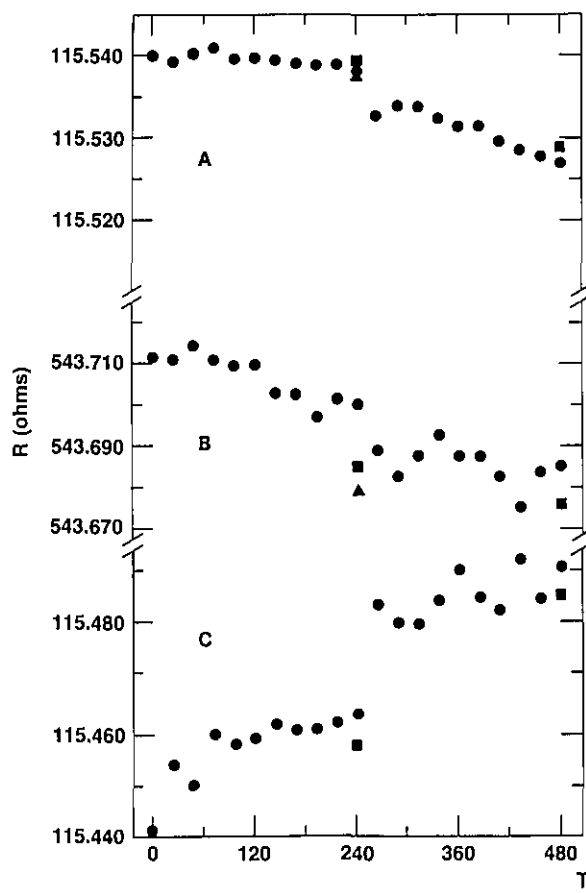
Figure 4—(Below)Variation of the resistances R of 6 IPRTs with heat treatment. Figure 4D gives the results for PC2/40 of sets III and IX; figures 4A, 4B, 4C, 4E, and 4F show the results for IPRTs PA10/25, PA2/22, PD2002/21, PA1001/48, and RD4/11, respectively, of sets VI and X. Measurements on these 6 IPRTs were made at 0 °C, 20 °C, 40 °C, 60 °C, 80 °C, and 100 °C, but only those at 40 °C are shown here. Time 0 refers to the original calibrations of IPRTs of sets III and VI prior to heat treatment. The • represents data for the original calibrations and those obtained after heat treatment. The ■ represents data of a measurement sequence performed after a preceding sequence, but without an intervening heat treatment; the ▲ represents data of the intital measurement sequence performed on sets IX and X.

310

time the studies of sets III and VI were completed and those of sets IX and X were begun. The behavior of the other three was unaffected by time at room temperature.

The magnitude of the change in calibration (drift) for each of the IPRTs investigated from the various companies is given in table 4. The mean values of the calibration drifts for the IPRTs of each company were calculated 1) by considering all of the IPRTs of sets I through X, 2) by considering all of the IPRTs of sets III through X, 3) by considering the IPRTs of sets III through X, but omitting the values of those IPRTs that are considered to be outliers in those sets, and 4) by considering the IPRTs of sets III through X, but omitting the values of those IPRTs that are repeats and those considered to be outliers in those sets. These data are depicted graphically by the histograms of figures 5, 6, and 7. Figure 5 shows the results of the 92 IPRTs that did not fail plus the results for those six IPRTs of sets IX

Table 4. IPRT calibration drift in mK. Underlined numbers in sets IX and X are the numbers for the IPRTs which had been previously measured in sets III and VI

Company	Set I	Set II	Set III	Set IV	Set V	Set VI	Set VII	Set VIII	Set IX	Set X
A	0	5	5	225	27	23		0	28	2
	7	2	8	25	18	17		0	20	0
	6				0	100		10	0	7
	0				20	8		8	35	7
	0				25	13			100	<u>0</u>
	8					0			0	<u>26</u>
	5					15			20	<u>4</u>
	5								4	
									11	

Mean for Sets I—X=18 (for 46 entries); 19 (for 43 entries, ignoring the 3 outliers).
Mean for Sets III—X=22 (for 36 entries); 24 (for 33 entries, ignoring the 3 outliers).
Mean for Sets III—X=12 (for 33 entries, ignoring 3 repeats); 12 (for 30 entries, ignoring 3 repeats and 3 outliers).

Company	Set I	Set II	Set III	Set IV	Set V	Set VI	Set VII	Set VIII	Set IX	Set X
A			55	20			58		33	
				25			16		38	
				10			35			
				2			0			
				8			10			
				40			120			
				25			28			
							15			
							117			

Mean for Sets III—X=34; 25 (ignoring 2 outliers).

Company	Set I	Set II	Set III	Set IV	Set V	Set VI	Set VII	Set VIII	Set IX	Set X
C			20		10		15	0	<u>8</u>	
			12					14		
			900							

Mean for Sets III—X=122 (for 8 entries); 11 (for 7 entries, not counting outlier).
Mean for Sets III—X=12 (for 6 entries, ignoring repeat and outlier).

Company	Set I	Set II	Set III	Set IV	Set V	Set VI	Set VII	Set VIII	Set IX	Set X
D			0	250	Open	30		Bad		<u>18</u>
			3	45	250	65		15		<u>10</u>
			0		8	15				
			5							

Mean for Sets I—X=51 (for 14 entries); 57 (for 12 entries, ignoring open circuit, bad IPRT, and 2 repeats).
Mean for Sets III—X=71 (for 10 entries); 85 (for 8 entries, ignoring open circuit, bad IPRT, and 2 repeats).
Mean for Sets III—X=26 (for 8 entries, ignoring open circuit, bad IPRT, and 2 outliers); 30 (for 6 entries, ignoring open circuit, bad IPRT, 2 outliers, and 2 repeats).

Company	Set I	Set II	Set III	Set IV	Set V	Set VI	Set VII	Set VIII	Set IX	Set X
E	0	1	0	20	8					26
	0	5	0	0						
		7								
		0								

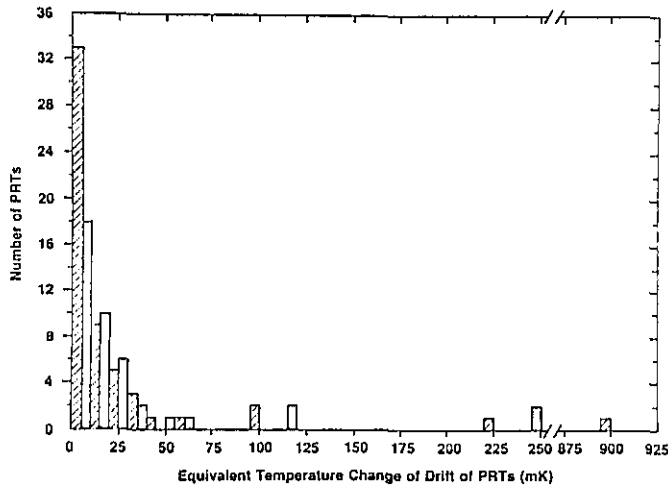Mean for Sets I—X=6.
Mean for Sets III—X=11.

Figure 5—Histogram of the drifts of all 98 IPRTs of sets I through X that did not fail during the investigation of their stability.

Figure 6—Histogram of the drifts of all 78 IPRTs of sets III through X that did not fail during the investigation of their stability.
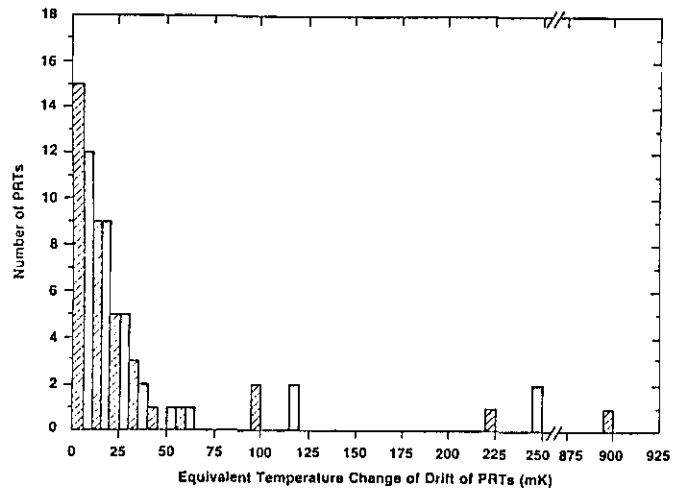

Figure 7—Histogram of the drifts of the 72 IPRTs of sets III through X that did not fail during the investigation of their stability and that excludes the 6 IPRTs of sets IX and X that had been examined previously in sets III and VI.
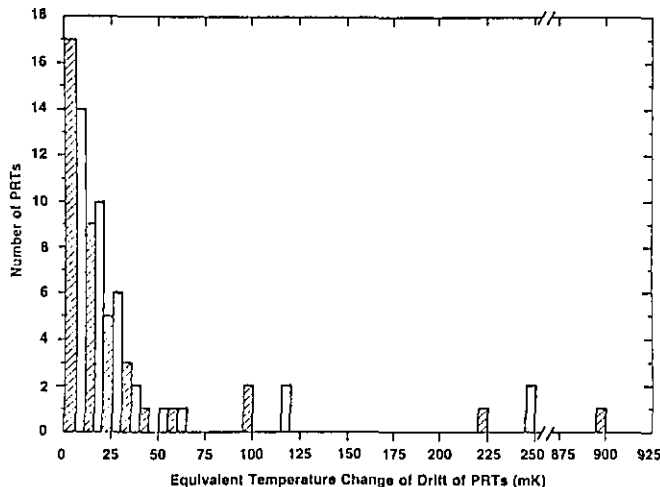
and X that were studied previously in sets III and VI, i.e., there are 98 entries. Figure 6 shows the results for the IPRTs of sets III through X that did not fail and includes the six IPRTs of sets IX and X that were studied also in sets III and VI, i.e., there are 78 entries. Figure 7 displays the results for the IPRTs of sets III through X that did not fail but it does not contain the results for those IPRTs of sets IX and X that had been studied previously in sets III and VI, i.e., there are 72 entries.

The calibration drifts of the IPRTs of sets I and II given in table 4 may be unusually small as a result of having had 15 prior heat treatments for a total time at 235 °C of about 186 hours. As can be seen from figures 1, 2, 3, and 4, such heat treatments could cause the IPRTs to become more stable, although some of the IPRTs of the other sets also had small drifts without the benefit of the additional time spent at 235 °C.

When the resistance data measured at 0 °C, 20 °C, 40 °C, 60 °C, 80 °C and 100 °C for each IPRT were plotted as a function of the time that the IPRT was kept at 235 °C, the scatter of the points about a smooth line through them was as follows: One IPRT had a scatter in resistance equivalent to ±15 mK, one of ±12 mK, two of ±10 mK, three of ±6 mK, and all others of the 90 of the 94 IPRTs that did not fail or have enormous changes in resistance had a scatter of ⩽±5 mK, with the majority of the latter having a scatter of from ±3 mK to ±5 mK.

Three IPRTs, one from each of three different models, from manufacturer A exhibited more change in resistance upon heat treatments than those of other models obtained from that company. Other IPRTs of those same three models, however, did not show such large changes. For the products of manufacturer B, the IPRTs of one model definitely had greater changes in resistance with heat treatments than did those of the other models. For manufacturer C, one model, for which there was only one IPRT, was considerably less stable than the other models upon heat treatments. One should not be hasty in drawing conclusions from this since that IPRT may not be representative of its model. For manufacturer D, the IPRTs of one model definitely appeared to be more unstable to changes in resistance with heat treatments than those of the other models of this company. Also, one IPRT of another model became

312

open circuit and another IPRT of yet a different model had a very large change in resistance. Not all IPRTs of the latter model exhibited such large changes, however. All models of manufacturer E appeared to be quite good, although one model, for which there was only one IPRT involved in the investigation, may have been marginally less stable than the other models.

Since the ice-point resistance value of an IPRT is determined essentially by the diameter of the platinum wire of which the sensor is made, one might expect the stability of the thermometers to be a function of their R_0 values. From our results, however, there does not appear to be any correlation between resistance value and stability upon heat treatment and handling. Of course, the IPRTs were heated to only about 235 °C, a relatively low temperature, so a dependence of the stability of the thermometers on resistance might develop if the sensors were heated to elevated temperatures.

About 90% of the IPRTs investigated exhibited hysteresis over the temperature range in which they were tested, i.e., over the range from 0 °C to 100 °C. We attribute this hysteresis to the presence of either strains in the platinum wire which forms the sensing elements or of moisture inside the encapsulation of the IPRTs.

Normally the IPRTs were heat-treated following the completion of a set of resistance measurements over the range from 0 °C to 100 °C. The heat treatment would be followed then by another set of resistance measurements at the same temperatures at which the IPRTs were tested before heat treatment. When, however, a measurement sequence was followed by another measurement sequence without the intervening heat treatment, 65 IPRTs (about 69%) had resistances at each temperature of measurement that were smaller than those measured in the previous sequence of measurements. Furthermore, when, following conditioning of the IPRTs at 235 °C, the resistances of the thermometers were measured at 0 °C, 20 °C, 40 °C, 60 °C, 80 °C, and 100 °C, and then the IPRTs measured in the reverse sequence, the measured resistance values at any given temperature of the reverse sequence were less than those obtained in the previous sequence at the same temperature. At any given temperature, the resistances continued to decrease with repeated sequential measurements, especially if the IPRTs were exposed to 0 °C between the sequences. This behavior was interpreted as being the result of increased shunting of the platinum sensing element by the presence of moisture. In order to test this hypothesis, thermal cycle 21 of set II proceeded in the normal manner, i.e., heat treatment of the IPRTs at 235 °C for 24 hours and then measurement of their resistances at the test temperatures of 0 °C, 20 °C, 40 °C, 60 °C, 80 °C, and 100 °C. Then, in what is called

cycle 21B, the resistances of the IPRTs were measured at 40 °C, and then at 0 °C. Measurements similar to those of cycle 21B were made in cycles 21C and 21D. The measurements were discontinued after measurements at 40 °C of cycle 21E. Some typical results of those tests are shown in figure 8. Some of the IPRTs exhibited total changes equivalent to 35 mK in these tests.
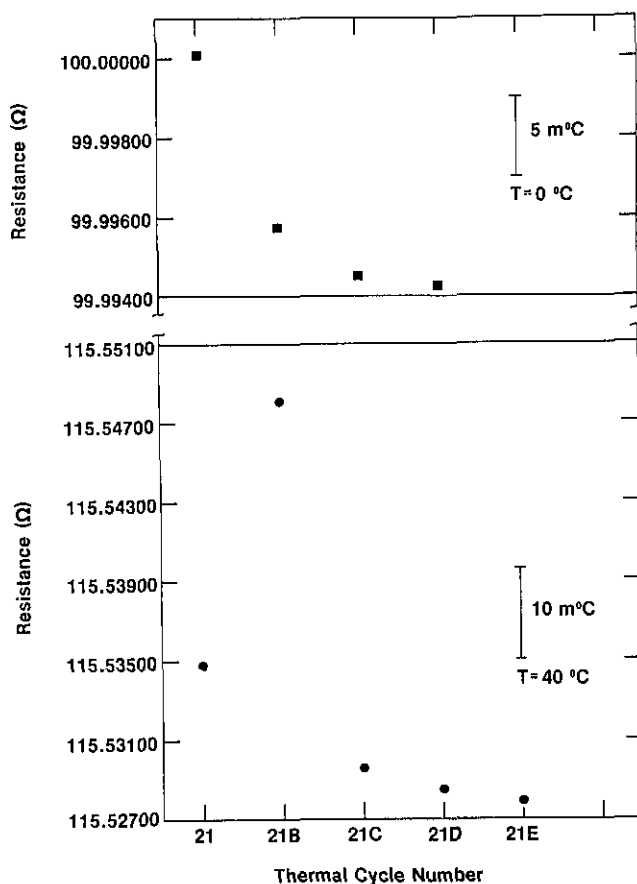

Figure 8—Results of the test for the presence of moisture in IPRT RD6/72. Sensor cycled between 40 °C and 0 °C. See text for elaboration.

It is believed that these tests showed that the resistance decreases were due to shunting as a result of "wetness." Note the large differences in the resistance at 40 °C of cycle 21B from those of thermal cycles 21 and 21C. This indicates that an appreciable amount of moisture was driven off the platinum element and its lead-wires during the calibration process of cycle 21 (measurements at 0 °C, 20 °C, 40 °C, 60 °C, 80 °C, and 100 °C) but that it recondensed during further measurements at 0 °C of cycle 21B. The elimination or the reduction of shunting (by the moisture) as a result of heating during the calibration process was possibly demonstrated also by some IPRTs which showed progressively less change in resistance at increasingly

313

higher test temperatures as a function of time at 235 °C (see fig. 2). That is to say, the change in resistance with time at 235 °C was considerably less at the higher test temperatures than it was at the lower temperatures.

When a measurement sequence was followed by another measurement sequence without an intervening heat treatment, 18 IPRTs exhibited evidence of strain of the platinum elements. This was manifested by increased resistances at the test temperatures.

Eighty-three IPRTs showed effects of either moisture or strain. The magnitudes of these effects and the distribution among the manufacturers of the IPRTs showing these effects are given in table 5. Only nine of the 92 IPRTs that did not fail during our investigation were free of moisture or strain effects. The magnitudes of the effects, expressed as equivalent temperature changes, are those maximum values obtained by comparing the results of a calibration at the six test temperatures with those of the preceding calibration without an intervening heat treatment.

Figure 9 shows the results of a dry and unstrained IPRT, RD7/73. The behavior depicted in this figure is to be compared with that of the IPRTs that exhibit the effects of moisture, such as that shown in figure 8 for IPRT RD6/72.
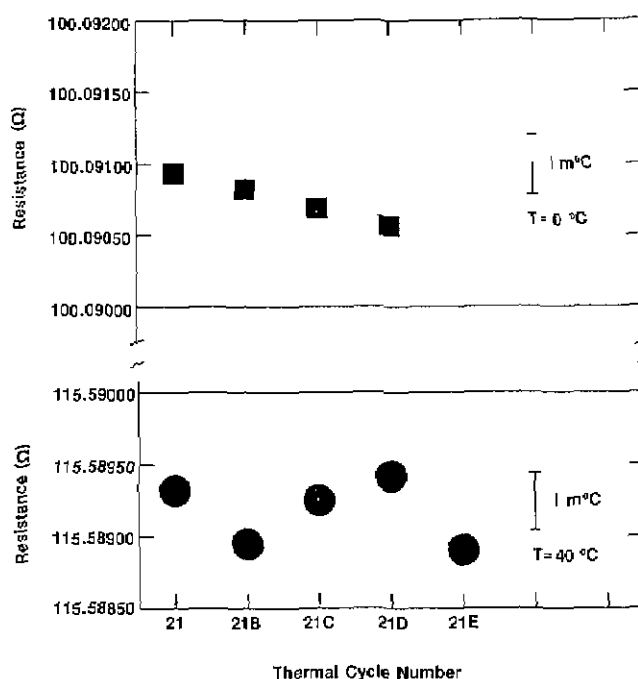

Figure 9—Results of the test for the presence of moisture in IPRT RD7/73. Sensor cycled between 40 °C and 0 °C. See text for elaboration.

Table 5. Effects of moisture and strain on IPRTs. Underlined numbers are the numbers of sets IX and X which had been previously measured in sets III and VI

Manufacturer	Dry and no strain, Sets I-X	Total number of IPRTs from each manufacturer	Number of IPRTs showing effects of moisture	Number of IPRTs showing effects of strain	Magnitude of effect (equivalent temperature changes) Moisture (mK)	Strain (mK)
A	6	43	23	14	15, 17, 10, 10, 10, 10, 17, 16, 6, 10, 3, 15, 8, 5, 5, 5, 8, 8, 10, 10, 7, 4, 2	15, 5, 5, 5, 3, 8, 4, 3, 4, 3, 2, 1, 3, 2
B	0	19	17	2	10, 5, 10, 10, 7, 10, 15, 3, 6, 5, 2, 18, 12, 8, 9, 4, 4	2, 1
C	2	7	3	2	12, 0, 2	3, 2
D	1	14 (1 bad and 1 open)	11	0	20, 13, 25, 1, 8, 12, 10, 3, 10, 0, 10	
E	0	11	11	0	10, 5, 3, 13, 13, 10, 3, 1, 10, 10, 14	
Total	9	94	65	18		
Percent	9.6%	(1 bad and 1 open) 2.1%	69.15%	19.15%		

The ice-point resistances, R_0, of most of the IPRTs varied with the time spent at 235 °C, as did the resistances at the other test temperatures. The magnitude of the changes in the R_0 values of the IPRTs varied by the equivalent of from 5 mK or less to more than 3 K. The maximum changes in R_0, expressed as the equivalent temperature changes, are given in the histogram shown in figure 10. The results shown in this figure are comprised of those of the IPRTs of sets I through X that did not fail and the histogram includes results of the six IPRTs of sets IX and X that had been tested previously in sets III and VI. Figure 11 is the histogram of the
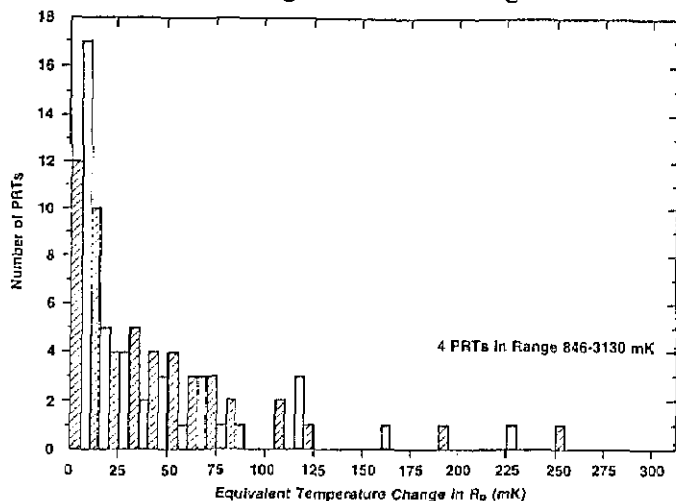

Figure 10 — Histogram of the maximum change in R_0 incurred by the 98 IPRTs of sets I through X that did not fail during tests of their stability upon heat treatment and handling. The change in R_0 is expressed as the equivalent change in temperature.
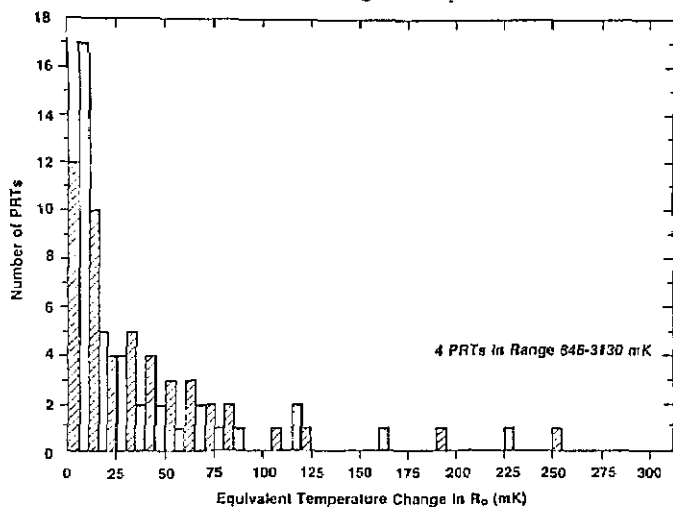

Figure 11 — Histogram of the maximum change in R_0 incurred by the 92 IPRTs of sets I through X, excluding the 2 IPRTs that failed and the 6 IPRTs of sets IX and X that had been tested previously in sets III and VI, during tests of their stability upon heat treatment and handling. The change in R_0 is expressed as the equivalent change in temperature.

results of the IPRTs of sets I through X that did not fail but it does not include the results of the six IPRTs of sets IX and X that had been tested previously in sets III and VI. With reference to figure 11, one can see that 39 IPRTs (42%) had changes in R_0 of the equivalent of 15 mK or less; 48 IPRTs (52%) had changes in R_0 of the equivalent of 25 mK or less; 65 IPRTs (71%) had changes of the equivalent of 50 mK or less; and 12 IPRTs (13%) had changes of the equivalent of greater than 100 mK.

With the exception of some of the IPRTs noted earlier in the discussion of the effects of moisture, the changes in R_0 with time spent at 235 °C have the same apparent general behavior as the changes in the resistances at the other test temperatures (see figs. 1—4). Consequently, one might expect that the ratio of the resistance at temperature t to the resistance at 0 °C, i.e., $R(t)/R_0 = W(t)$, would exhibit less change than just the resistance itself upon heat treatment and handling. That, however, was not found to be the case. There was no apparent improvement in the stability of the IPRTs when considering the $W(t)$ instead of the resistance.

Conclusions

The results from the 94 thermometers investigated in the study of the stability of IPRTs upon heat treatment and handling showed that there were no major differences among the products of the different manufacturers, although manufacturer D had an exceptionally high percentage of IPRTs that either failed or exhibited very large changes in resistance. This, however, may have been fortuitous. Manufacturers B and D each had one model of IPRTs that definitely appeared to be less stable than the products of their other models. Only 12 IPRTs (13%) were stable to 5 mK or less upon heat treatment; thus, most of the IPRTs exhibited calibration drift and effects due to the presence of moisture or strain. Wetness definitely is a problem with IPRTs and the magnitude of the effect can be ascertained only by experiments designed to test for its presence. There does not appear to be any advantage in obtaining the resistance ratio, $W(t)$, as a way of increasing measurement precision.

Before an IPRT is put into use at almost any level of precision and accuracy, it should be tested for calibration drift and it should be tested at a temperature other than the ice point, unless it is to be used at 0 °C or below. Also, if an inaccuracy of $\leqslant \pm 30$ mK is needed, the IPRT should be tested for the presence of moisture. Notwithstanding the calibration drift and the possibility of the presence of moisture or strain, IPRTs should be excellent for use in temperature control at a fixed temperature which is greater than about 5 °C.

References

[1] Carr, K. R. An Evaluation of Industrial Platinum Resistance Thermometers, in *Temperature, Its Measurement and Control in Science and Industry*, (Instrument Society of America, Pittsburgh, 1972), Vol. 4, Part 2, pp. 971-982.

[2] Quinn, T. J. Report on the Examination of Industrial Platinum Resistance Thermometers, Proces Verbaux du CCT, Document No. CCT/73-65, 1973.

[3] Sinclair, D. H.; H. G. Terbeek and J. H. Malone, Calibration of Platinum Resistance Thermometers, in *Temperature, Its Measurement and Control in Science and Industry*, (Instrument Society of America, Pittsburgh, 1972), Vol. 4, Part 2, pp. 983-988.

[4] Chattle, M. V. Resistance Ratio/Temperature Relationships for Industrial Platinum Resistance Thermometers, NPL Report QU (U.K. Natl. Phys. Lab., Div. of Quantum Metrol.), QU 30, 1975, 18 pp.

[5] Chattle, M. V. Resistance Ratio/Temperature Relationships for Industrial Platinum Resistance Thermometers of Thick Film Construction, NPL Report QU (U.K. Natl. Phys. Lab., Div. of Quantum Metrol.), QU 42, 1977, 11 pp.

[6] Actis, A. and L. Crovini, Interpolating Equations for Industrial Platinum Resistance Thermometers in the Temperature Range from −200 to +420 °C, in *Temperature, Its Measurement and Control in Science and Industry*, (American Institute of Physics, New York, 1982), Vol. 5, Part 2, pp. 819-827.

[7] Bass, N. M. Construction of a Laboratory Working Thermometer Using Industrial Platinum Resistance Sensors, in *Temperature, Its Measurement and Control in Science and Industry*, (American Institute of Physics, New York, 1982), Vol. 5, Part 2, pp. 813-814.

[8] Connolly, J. J. The Calibration Characteristics of Industrial Platinum Resistance Thermometers, in *Temperature, Its Measurement and Control in Science and Industry*, (American Institute of Physics, New York, 1982), Vol. 5, Part 2, pp. 815-817.

[9] Curtis, D. J. Thermal Hysteresis and Stress Effects in Platinum Resistance Thermometers, in *Temperature, Its Measurement and Control in Science and Industry*, (American Institute of Physics, New York, 1982), Vol. 5, Part 2, pp. 803-812.

[10] McAllan, J. V. Practical High Temperature Resistance Thermometry, in *Temperature, Its Measurement and Control in Science and Industry*, (American Institute of Physics, New York, 1982), Vol 5, Part 2, pp. 789-793.

[11] Mangum, B. W. and G. A. Evans, Jr., Investigation of the Stability of Small Platinum Resistance Thermometers, in *Temperature, Its Measurement and Control in Science and Industry*, (American Institute of Physics, New York, 1982), Vol. 5, Part 2, pp. 795-801.

[12] Riddle, J. L.; G. T. Furukawa and H. H. Plumb, Platinum Resistance Thermometry, National Bureau of Standards (U.S.) Monograph 126, 1973 (Superintendent of Documents, U.S. Government Printing Office, Washington, DC 20402).

[13] A simplified version of this bridge is described in detail in the paper of ref. 14.

[14] Brown, N. L.; A. J. Fougere, J. W. McLeod, and R. J. Robbins, An Automatic Resistance Thermometer Bridge, in *Temperature, Its Measurement and Control in Science and Industry*, (American Institute of Physics, New York, 1982), Vol. 5, Part 2, pp. 719-727.

[15] Comptes rendus des séances de la Quinzième Conférence Générale des Poids et Mesures, Resolution 7, p. 105, Annexe 2, p. A1(1975); Also, Metrologia 12, 7 (1976).

Thermal Expansion of Liquid Normal Hydrogen Between 18.8 and 22.2 K

L. A. Schwalbe and E. R. Grilly

Los Alamos National Laboratory, Los Alamos, NM 87545

The thermal expansion coefficient α of liquid normal hydrogen (n-H_2) was measured between 18.8 and 22.2 K in the pressure range 5 to 70 bar. The results are compared with those derived from PVT measurements by others on both normal and *para* (p-H_2) hydrogen. Our analysis of the earlier normal data includes fitting an empirical equation of state, and expansion coefficients are derived from this equation by differentiation. We discuss the effects on α and the compressibility β from molecular quadrupole interactions; both theoretical and empirical results suggest these to be on the order of 2% or less for the normal spin mixture. We conclude that our thermal expansion data are consistent with earlier results on both n-H_2 and p-H_2 in this range of pressures and temperatures.

Key words: hydrogen, normal; hydrogen, *para*; pressure, 5 to 70 bar; temperature, 18.8 to 22.2 K; thermal expansion coefficient.

1. Introduction

The prototype, inertial-confinement reactor, designed and built at this laboratory, is fueled with mixtures of D_2, DT, and T_2. The fuel is contained in tiny (100 μm diameter), hollow glass microballoons. Its state is either solid or liquid depending on the temperature and pressure, which are fixed somewhere in the range between 18.5 and 23.0 K, and zero and 70 bar.

When the program for target fabrication began, little was known about the behavior of the fuels. Therefore, along with other work, efforts were included to measure and correlate the physical properties of all the hydrogen isotopes. Our part in this program has been to supply thermodynamic data on the solid and liquid phases. One product of this research is a recently published study on deuterium [1][1]. Similar data on tritium will follow. Here,

we consider the equation of state for liquid H_2 with particular emphasis on the thermal expansivity α of the normal spin mixture.

In this range of temperature and pressure the properties of liquid *para* hydrogen (p-H_2) are well described [2,3]. PVT data exist [4] for normal hydrogen (n-H_2), which contains 0.25 *para* ($J=0$) and 0.75 *ortho* ($J=1$) species. While the latter results are less extensive, the combined data are sufficient to describe certain differences between n-H_2 and p-H_2 such as the 0.5% difference in their molar volumes [5]. Usually, the liquid thermal expansion and compressibility β are assumed to be independent of the *ortho-para* composition. Theoretical estimates, discussed below, suggest that the differences, $\Delta\alpha=\alpha(n$-$H_2)-\alpha(p$-$H_2)$ and $\Delta\beta=\beta(n$-$H_2)-\beta(p$-$H_2)$, are about 2%.

Our purpose is to examine the effects of the *ortho-para* composition explicitly. We show that compressibilities derived from earlier PVT measurements of n-H_2 and p-H_2 are consistent with theoretical estimates of $\Delta\beta$. However, the precision of these data is not sufficient to permit a similar analysis for $\Delta\alpha$. It was, therefore, necessary to measure the expansivity of n-H_2 directly. These data, presented below, range in temperature from 18.8 to 22.2 K and in pressure from about 5 to 70 bars. We compare them with earlier data on both p-H_2 [3] and

---

---

[1]Figures in brackets indicate literature references at the end of this paper.

n-H$_2$ [4], and find the results to be generally consistent with theory.

2. Experimental

The experiments on liquid hydrogen were carried out with the same apparatus as that described and used in the previous work on deuterium [1]. Briefly, the pressure cell consisted of three BeCu diaphragms welded together at their circumference and separated by 0.3 mm gaps. The upper gap, which served as the sample chamber, could be sealed with a low-temperature valve; the lower gap remained open to a room-temperature gas-handling system.

The entire pressure-cell assembly was held immersed in a bath of liquid hydrogen. Temperatures were obtained from measurements of the vapor pressure of the cryogen and the liquid-vapor equation for p-H$_2$ by Souers et al. [6]. (By strict definition our cryogen was not pure *para*; the equilibrium mixture of hydrogen at this temperature, commonly denoted as e-H$_2$, contains an *ortho* fraction of about 0.2%. However, for the following discussion the difference between e-H$_2$ and p-H$_2$ is insignificant, and both forms will be referred to simply as p-H$_2$.)

The volume of the sample is determined by the deflections of the upper and middle diaphragms of the cell. Increased internal pressures P_u in the upper gap increase the sample volume V_u. Increased external pressures, either in the lower gap P_l or in the surrounding cryogen bath P_b, decrease V_u. These impressed changes are expressed quantitatively by

$$\Delta V_u = (S_u + S_l)\Delta P_u - S_l \Delta P_l - S_u \Delta P_b \qquad (1)$$

where S_u and S_l are pressure sensitivity factors of the volume to changes in the upper and middle diaphragm displacements, respectively. The sensitivity factors were determined by calibrating the sample volume at $T = 20.00$ K against the density values for p-H$_2$ tabulated by Goodwin et al. [2].

There is no explicit temperature dependence included in eq (1). In this range, there should be negligible effects from the thermal expansion of the cell material. To our knowledge, there are no measurements of thermal expansion for beryllium-copper, but data for copper exist, and the temperature coefficient for the alloy should be comparable. Rubin et al. [7] reported a linear expansion coefficient of 6×10^{-6} for copper at 25 K. Between 19 and 22 K, the volume coefficient should, therefore, be somewhere between 1 and 2×10^{-5} K^{-1}. The results obtained in this range for α of liquid hydrogen are between 9 and 19×10^{-3} K^{-1}. If accuracy limits for the

hydrogen data are set at about 1%, the effects of thermal expansion from the cell are at least an order of magnitude lower than the uncertainties arising from other sources.

To begin a set of measurements at a given pressure, the sample chamber was first evacuated, then filled with hydrogen, and sealed with the valve. Typically, during each run the temperature was first decreased and then increased in increments of 0.4 K. Each experimental value for α was obtained from the measured change in the lower-cell pressure ΔP_l that was required to maintain constant sample pressure P_u when the temperature of the system was changed by an amount ΔT. From eq (1) it follows that

$$\alpha = \frac{1}{V}\left(\frac{\partial V}{\partial T}\right)_P = -\frac{S_l \Delta P_l}{\bar{V}_u \Delta T} - \frac{S_u}{\bar{V}_u}\left(\frac{dP_b}{dT}\right) \qquad (2)$$

where $\bar{V}_u$ is the average sample volume for the measurement, and dP_b/dT is the temperature derivative of the cryogen vapor pressure calculated from the Souers et al. [6] equation for liquid p-H$_2$.

The total time of each sample confinement at low temperatures was about 12 or 13 h although one sample was kept cold for as long as 100 h. During the course of each set of measurements there was some *ortho*-to-*para* conversion. Our data were, therefore, not taken on "normal hydrogen" in the strictest sense. But the starting material for each sample was n-H$_2$, and we estimate the *ortho* fractions of most samples to have been in the range 0.65 to 0.75 at the time of their measurement.

The time for temperature equilibration at each point varied between 20 and 90 min depending on the amount of cryogen in the bath. During the course of each measurement, the effects of *ortho*-to-*para* conversion were, therefore, about 1 or 2%. Because this amount is roughly equal to the accuracy limits of the data, we corrected all of the measurements for conversion. The correction procedure begins by estimating $x_0(t)$, the *ortho* fraction of the sample at the time of the measurement. An expression for this is obtained by integrating the rate equation

$$\frac{dx_0}{dt} = -0.019\,x_0^2\,\text{h}^{-1}, \qquad (3)$$

which had been determined from previous measurements in the cell at 15 K and 30 bar using gaseous thermal conductivity [8] for the x_0 determination. The rate constant is somewhat greater than the value, 0.0114 h^{-1}, given by Woolley et al. [9]. The integration constant, $x_0(0) = 0.75$, is set by assuming the normal spin mixture at the time of the sample loading. The calcu-

318

lated *ortho* fraction in eq (3) gives the rate of conversion, which we multiply by the duration of each measurement and by $\Delta V/V \Delta x_0 = 7.4 \times 10^{-3}$. The latter value was derived from the data of Scott and Brickwedde [5] and checked by direct measurements in this cell at 15 K and 34 bar.

The results of this work are listed in table 1. Included with them are 14 additional data (mostly on p-H_2), which were taken about 18 months before the main study on n-H_2. We estimate the accuracy of the expansion data to be about ± 1or 2%. For comparison with results of others, we have also plotted the n-H_2 data in figure 1. The solid lines in the plot represent interpolated values for α of p-H_2 from the work of Roder et al. [3]. The dashed lines were derived from an equation of state fitted to the PVT data that Johnston et al. [4] reported for n-H_2.

3. Discussion

3.1 Comparison with Earlier Liquid n-H_2 Data

Of the existing PVT work on liquid n-H_2, that of Johnston et al. [4] is the most useful for present comparisons. Their data were taken along seven isotherms between 20.3 and 32.6 K. Temperatures were measured with a copper-constantan thermocouple calibrated against the vapor pressure equation for n-H_2 by White et al. [10].

The pressure cell used in the PVT experiment contained a constant, known volume of sample. The molar volume along each isotherm was determined by first filling the cell to the highest pressure (ca. 100 bar) and then decreasing the pressure in steps of about 10 or 20 bar. After each decrease in pressure, measurements were made of the amount of material drawn from the cell. When the sample pressure had been lowered to about 10 bar, the entire quantity of remaining liquid was measured to establish absolute molar volumes for the isotherm. We estimate a relative precision of $\pm 0.03\%$ for volume data within each set at constant temperature. The absolute accuracy of the measurements is probably about $\pm 0.15\%$.

Johnston et al. [4] found their PVT results well represented by an equation of the form

$$P = A_v + T\,B_v \tag{4}$$

where A_v and B_v are functions of the molar volume only. They gave the following analytical expression for B_v:

Table 1. Measurements of the thermal expansivity of liquid hydrogen.

T(K)	P(bar)	x_0	$\alpha(10^{-3}K^{-1})$	T(K)	P(bar)	x_0	$\alpha(10^{-3}K^{-1})$	T(K)	P(bar)	x_0	$\alpha(10^{-3}K^{-1})$
22.0	5.48	0.42	18.86	20.4	28.52	0.69	12.32	21.6	56.05	0.53	10.96
21.6	5.48	0.42	17.63	20.8	28.52	0.69	12.65	21.2	56.05	0.53	10.74
21.2	5.48	0.42	17.12	22.0	28.52	0.53	13.75	20.4	69.81	0.73	9.58
22.1	5.48	0.31	18.42	21.6	28.52	0.53	13.34	20.0	69.81	0.72	9.48
21.9	5.48	0.31	18.12	21.2	28.52	0.53	13.07	19.6	69.81	0.72	9.24
21.7	5.48	0.31	17.64	20.8	42.28	0.72	11.34	19.2	69.81	0.72	9.06
21.5	5.48	0.31	17.36	20.4	42.28	0.72	11.29	19.2	69.81	0.70	9.46
21.3	5.48	0.31	17.29	20.0	42.28	0.71	11.01	19.6	69.81	0.70	9.18
21.1	5.48	0.31	17.10	19.6	42.28	0.71	10.85	20.0	69.81	0.69	9.36
20.8	14.76	0.74	14.94	19.2	42.28	0.71	10.55	20.4	69.81	0.68	9.49
20.4	14.76	0.73	14.26	19.2	42.28	0.67	10.84	20.8	69.81	0.68	9.70
20.0	14.76	0.73	13.82	19.6	42.28	0.66	10.76	20.8	69.81	0.67	10.03
19.6	14.76	0.72	13.45	20.0	42.28	0.65	10.98	20.8	69.81	0.66	9.74
19.2	14.76	0.72	13.01	20.4	42.28	0.64	11.08	20.8	69.81	0.66	10.01
18.8	14.76	0.72	12.60	20.8	42.28	0.63	11.43	14.5	6.16	0.002	10.28[a]
18.8	14.76	0.69	12.76	20.8	56.05	0.74	10.73	15.5	6.16	0.002	11.03[a]
19.2	14.76	0.68	12.88	20.4	56.05	0.73	10.32	16.5	6.16	0.002	11.77[a]
19.6	14.76	0.67	13.25	20.0	56.05	0.73	10.12	14.4	15.43	0.02	9.69[a]
20.0	14.76	0.66	13.68	19.6	56.05	0.72	9.96	15.5	37.13	0.002	9.01[a]
20.4	14.76	0.65	14.10	19.2	56.05	0.72	9.70	16.5	37.13	0.002	9.44[a]
20.8	14.76	0.64	14.45	19.2	56.05	0.69	9.59	15.6	50.66	0.002	8.58[a]
20.8	28.52	0.74	13.20	19.6	56.05	0.68	9.83	15.6	50.66	0.02	8.51[a]
20.4	28.52	0.73	12.52	20.0	56.05	0.67	9.94	15.6	50.66	0.20	8.53[a]
20.0	28.52	0.73	12.22	20.4	56.05	0.66	10.07	16.5	69.81	0.002	8.01[a]
19.6	28.52	0.73	11.92	20.8	56.05	0.65	10.44	17.5	69.81	0.002	8.37[a]
19.2	28.52	0.73	11.63	21.2	56.05	0.72	10.62	18.5	69.81	0.002	8.69[a]
19.2	28.52	0.71	11.49	21.6	56.05	0.72	10.93	19.25	69.81	0.002	9.02[a]
19.6	28.52	0.70	11.82	22.0	56.05	0.72	11.26	19.75	69.81	0.002	9.32[a]
20.0	28.52	0.70	12.10	22.0	56.05	0.53	11.12				

[a]Measurements on liquid hydrogen taken about 18 months before the main study.
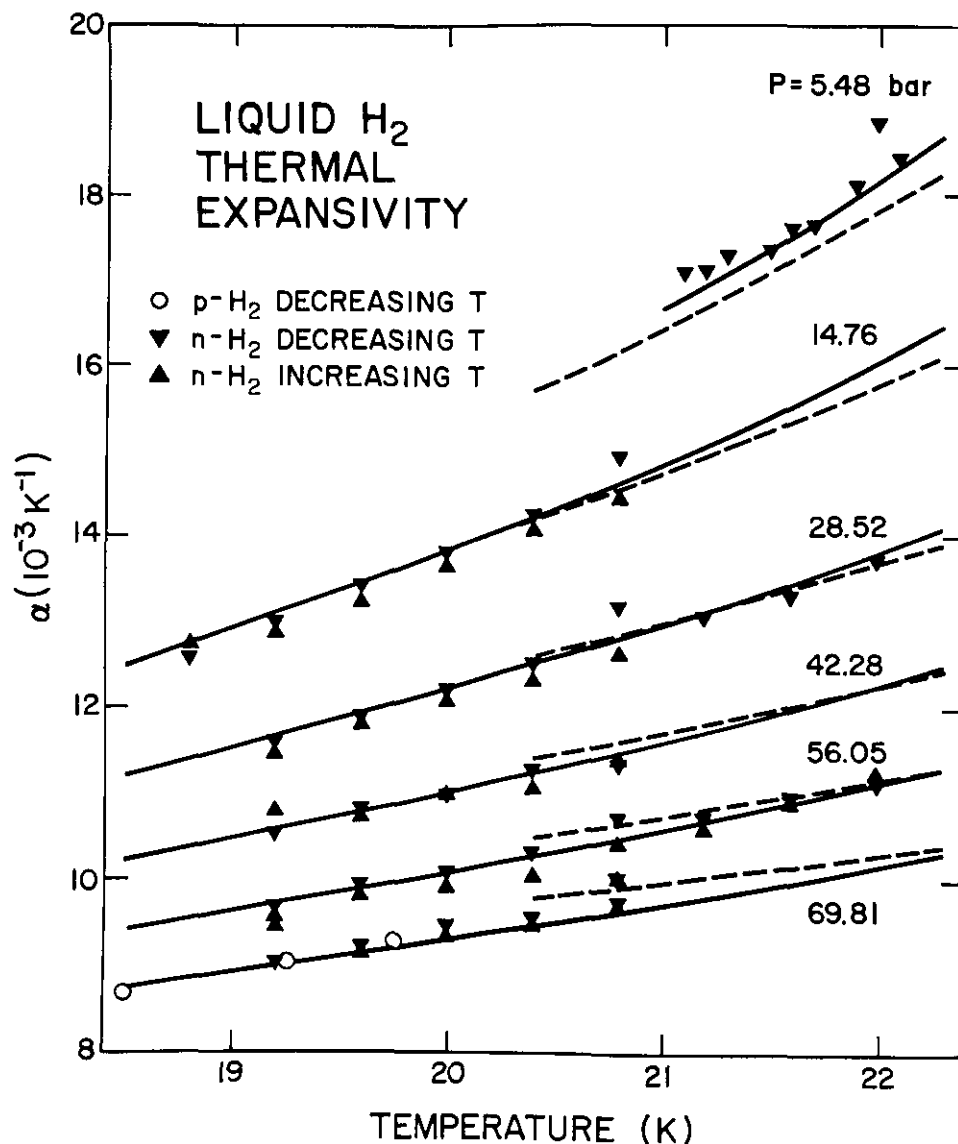
Figure 1 — Thermal expansion coefficient of liquid hydrogen. Solid lines represent values interpolated from the p-H_2 data of Roder et al. [3]. The dashed lines were obtained by differentiating eq (4) with B_v and A_v defined by eq (6). The parameter values were derived from a least-squares fit to the data of Johnston et al. [4].

$$B_v = -7.204 + \frac{442.8}{V} \qquad (5)$$

where V is taken in cm^3/mole and B_v is given in bar/K. The corresponding volume relationship of A_v appears in tabular form.

Thermal expansivities can be calculated from eq (4) by taking ratios of the temperature and volume derivatives of the pressure. To do this accurately, though, it is necessary to have both A_v and B_v expressed as analytic functions. We, therefore, fit low-order polynomials in both V and $1/V$ to the tabulated A_v data. Close fits were obtained with several different forms, but none of these curves when combined with eq (5) could accurately reproduce the PVT measurements.

Better results were obtained by fitting the original

PVT data to eq (4) with the following parametric functions:

$$B_v = a_1 + \frac{a_2}{V} \qquad (6a)$$

$$A_v = a_3 + \frac{a_4}{V} + \frac{a_5}{V^2} + \frac{a_6}{V^3}. \qquad (6b)$$

The analysis began by converting the original pressure units to bars and by adjusting the temperatures from the NBS-55 scale to the IPTS-68 [11]. A nonlinear least-squares fit then gave the following parameter values: $a_1 = -7.42290$, $a_2 = 4.53373 \times 10^2$, $a_3 = -3.19037 \times 10^2$, $a_4 = 5.67951 \times 10^4$, $a_5 = -3.02764 \times 10^6$, and

$a_6 = 0.435304 \times 10^8$. The standard and average absolute deviations of the volume measurements from the fitted equation of state are 0.033 and 0.085 cm^3/mole, respectively. The deviations are comparable to the $\pm 0.15\%$ accuracy limits estimated for these types of measurements [1]. Similar results are obtained by applying the same analysis to earlier data on liquid n-D$_2$ [12].

Thermal expansivities were calculated from eqs (4) and (6) at pressures corresponding to our isobars. The results, plotted in figure 1 as dashed lines, agree well with our measurements except at low pressures where the calculated values are smaller by about 3%. We regard the overall consistency to be quite satisfactory, particularly in view of the uncertainties expected in this type of analysis. The lowest temperature measurements that Johnston et al. made were at 20.329 K. Fitted functions, and especially quantities calculated from these by differentiation, are subject to large uncertainties near the endpoints of the data domain.

3.2 Comparison with Earlier Liquid p-H$_2$ Data

Goodwin et al. [2] published PVT measurements on liquid p-H$_2$. From these results Roder et al. [3] derived pressure functions of density at integral values of temperature. The latter report also contains tabulated values of temperature and density derivatives of the liquid pressure. We calculated thermal expansion coefficients from these tables and interpolated the results to our measured pressures. The calculations agree with our direct measurements on p-H$_2$. Also, as seen in figure 1 where the calculated values are plotted as solid lines, there is a close correspondence with our measurements on n-H$_2$.

Scott and Brickwedde [5] measured liquid volumes of both normal and *para* hydrogen along the vapor pressure curve below 20.4 K. The differences observed between the two data sets are well understood. Attractive forces among the *ortho* fraction introduce an effective pressure that reduces the molar volume V. To our knowledge, there are no direct measurements of molecular quadrupole effects on α or β, but it is instructive to consider

$$\ln V(n\text{-H}_2) \simeq \ln V(p\text{-H}_2) - \frac{\Delta V}{V(p\text{-H}_2)}, \qquad (7)$$

which is correct to first order in the absolute volume difference ΔV. Differentiation of eq (7) gives

$$\Delta\alpha \equiv \alpha(n\text{-H}_2) - \alpha(p\text{-H}_2) = -\frac{\partial}{\partial T}\left(\frac{\Delta V}{V}\right)_P \qquad (8a)$$

$$\Delta\beta \equiv \beta(n\text{-H}_2) - \beta(p\text{-H}_2) = \frac{\partial}{\partial P}\left(\frac{\Delta V}{V}\right)_T. \qquad (8b)$$

Figure 2 is a plot of $\Delta V/V$, the fractional volume difference between the n-H$_2$ data of Johnston et al. [4] and the interpolated smooth functions for p-H$_2$ by Roder et al. [3]. We believe the n-H$_2$ data are sufficiently precise that empirical estimates of $\Delta\beta$ can be obtained from this plot. In the noncritical regime all data follow the same general trend. The slope of the 20.4-K isobar, in particular, suggests that $\Delta\beta = -0.025 \times 10^{-3}$ bar^{-1}. For an average compressibility of 1.3×10^{-3} bar^{-1}, the effect is about 2%. We measured liquid compressibilities of both n-H$_2$ and p-H$_2$ at various pressures and temperatures and confirmed that $\Delta\beta$ is no larger than this amount. Similar estimates for $\Delta\alpha$ are not possible because of the inaccuracies involved in measuring the amounts of n-H$_2$ used in different sample loadings [4].

It is interesting to compare these empirical results with theoretical estimates of $\Delta V/V$. Driessen et al. [13] provide a prescription for calculating the effective pressure P_Q introduced by the electric quadrupole interactions of the *ortho* species. From this and the compressibility, the fractional change in the liquid volume is calculated from

$$\frac{\Delta V}{V} = -\beta\, P_Q. \qquad (9)$$

Although Driessen et al. [13] developed their formula to calculate fractional volume changes in the solid, we shall assume the procedure is valid for the liquid systems as well.

We calculated $\Delta V/V$ for liquid hydrogen along the five isotherms shown in figure 2. At low pressures the calculated isotherm at 20.359 K extrapolates to 5.6×10^{-3}, which agrees with the experimental result of Scott and Brickwedde [5]. At pressure, the calculated results are generally higher by about 2.5×10^{-3} than those found empirically. At 100 bar, for example, the theoretical values fall in the range 3 to 4×10^{-3}. Despite this difference the empirical and theoretical results are reasonably consistent. A discrepancy of 0.25% is roughly equal to the combined limits of error for the two liquid PVT experiments [3,4].

The slopes of the calculated $\Delta V/V$ versus P are qualitatively similar to those observed experimentally. In the noncritical regions, the calculated slopes are consistently smaller although probably not significantly so. The average theoretical $\Delta\beta$ indicated for the 20.359-K isotherm is about -0.018×10^{-3} bar^{-1}, compared to the experimental value -0.025×10^{-3} found above.

321

ΔV/V FOR LIQUID
n-H₂ AND p-H₂

- ● 20.339 K
- ○ 20.379 K
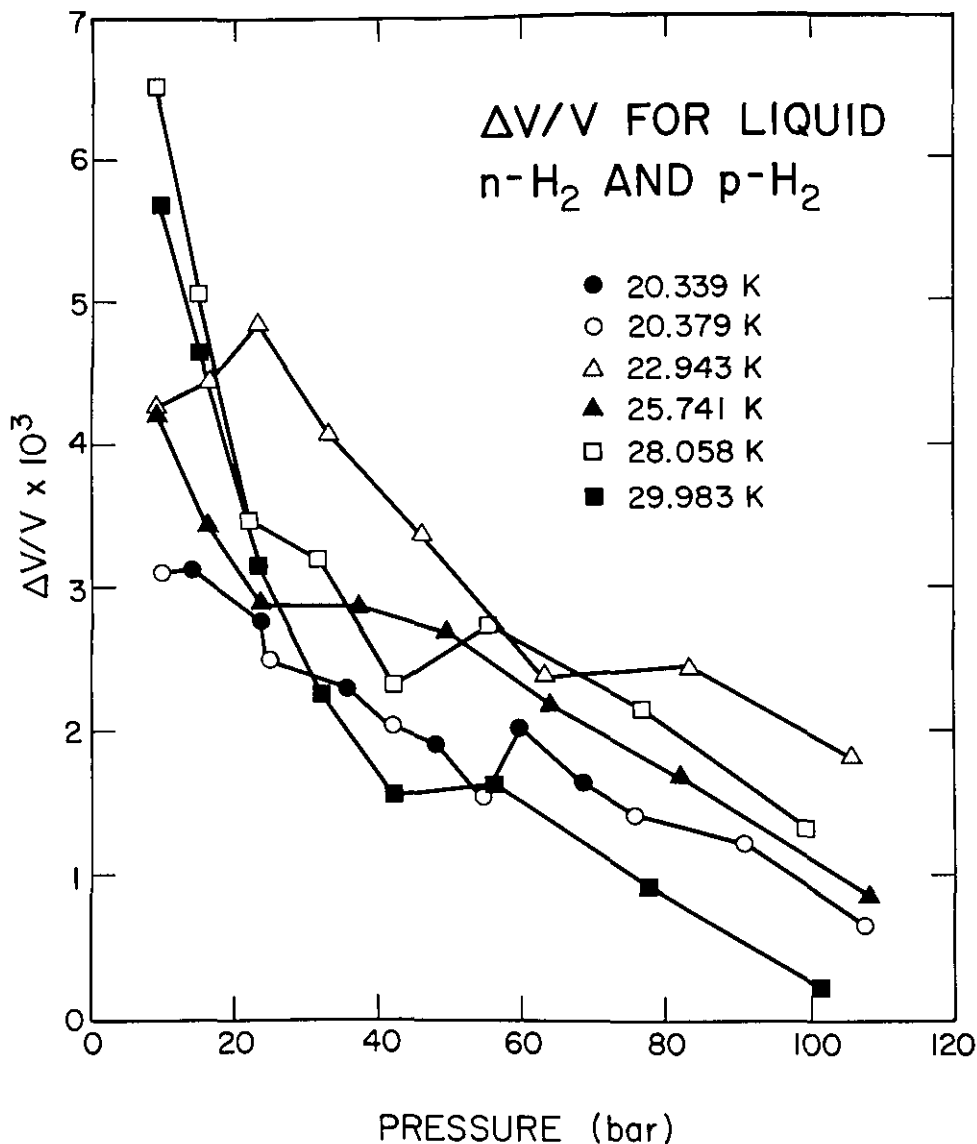- △ 22.943 K
- ▲ 25.741 K
- □ 28.058 K
- ■ 29.983 K

Figure 2—Plot of the fractional difference between the molar volumes of liquid normal and *para* hydrogen. The n-H_2 data were taken from [4]. The p-H_2 volumes were interpolated from the smooth curves of [3]. Isotherm *temperatures are given on the* IPTS-68.

PRESSURE (bar)

The difference between $\alpha(n$-$H_2)$ and $\alpha(p$-$H_2)$ can be calculated from eqs (8a) and (9). Resulting values for $\Delta\alpha$ are on the order of 0.10×10^{-3} K^{-1} or less in the temperature range 19 to 22 K for pressures below 20 bar. At higher presures, 40 to 80 bar, the difference increases to between 0.10 and 0.16×10^{-3} K^{-1}, which is still only about a 1.5% effect. If the empirical $\Delta\beta$ at higher temperatures suggests that our theoretical estimates for quadrupole effects on α and β are too small, even by a factor of two, the magnitude of $\Delta\alpha$ would still not exceed 2 or 3% for the range of temperatures and pressures of the present investigation. Therefore, within the combined limits of experimental error, the expansion data for p-H_2 agree with our direct results on n-H_2.

4. Summary and Conclusion

We measured thermal expansion coefficients of liquid normal hydrogen in the temperature range 18.8 to 22.2 K and at pressures between 5 and 70 bar. The data are corrected for volume changes due to *ortho-para* conversion. Included with the tabulated expansivity data are calculated estimates of the *ortho* fractions of the samples at the time of the measurements.

To compare our results with the n-H_2 data of Johnston et al. [4], we first converted the pressure units of the earlier data to bars and adjusted the temperatures to the IPTS-68. A least-squares fit defines an empirical

322

function for the liquid pressure. Thermal expansivities calculated from this function agree with present direct measurements except at the lowest pressures.

We discussed the effects of molecular quadrupole interactions among the o-H_2 fraction of the normal spin mixture. Comparisons between earlier data on normal [4,5] and *para* [3,5] hydrogen show that experimental $\Delta V/V$ are reasonably consistent with theoretical estimates based on the prescription of Driessen et al. [13]. Empirical and theoretical estimates of $\Delta\beta$ also agree; both suggest that quadrupole interactions decrease the compressibility by about 2%. Comparable estimates of $\Delta\alpha$ are not possible because of the inaccuracies in the n-H_2 data. However, calculated estimates in our temperature and pressure domain suggest that $\Delta\alpha$ is no larger than 2 or 3%. The observed agreement between our measured α on n-H_2 and corresponding p-H_2 data derived by Roder et al. [3] corroborate theoretical estimates of $\Delta\alpha$.

References

[1] Schwalbe, L. A., and E. R. Grilly, J. Res. Natl. Bur. Stand. (U.S.) **89**, 143 (1984).

[2] Goodwin, R. D.; D. E. Diller, H. M. Roder, and L. A. Weber, J. Res. Natl. Bur. Stand. (U.S.) **67**, 173 (1963).

[3] Roder, H. M.; L. A. Weber and R. D. Goodwin, Natl. Bur. Stand. Monograph 94 (Aug. 1965).

[4] Johnston, H. L.; W. E. Keller and A. S. Friedman, J. Am. Chem. Soc. **76**, 1482 (1954).

[5] Scott, R. B., and F. G. Brickwedde, J. Res. Natl. Bur. Stand. (U.S.) **19**, 237 (1937), J. Chem. Phys. **5**, 736 (1937).

[6] Souers, P. C.; C. K. Briggs, J. W. Pyper, and R. T. Tsugawa, Lawrence Livermore National Laboratory, Livermore, CA 94550, UCRL-52226 (1977).

[7] Rubin, T.; H. W. Altman and H. L. Johnston, J. Am. Chem. Soc. **76**, 5289 (1954).

[8] Grilly, E. R., Rev. Sci. Instrum. **24**, 72 (1953).

[9] Woolley, H. W.; R. B. Scott and F. G. Brickwedde, J. Res. Natl. Bur. Stand. (U.S.) **41**, 379 (1948).

[10] White, D.; A. S. Friedman and H. L. Johnston, J. Am. Chem. Soc. **76**, 1552 (1954).

[11] Bedford, R. E.; M. Durieux, R. Muijlwijk, and C. R. Barber, Metrologia **5**, 47 (1969).

[12] Friedman, A. S.; M. Trzeciak and H. L. Johnston [J. Am. Chem. Soc. **76**, 1552 (1954)] applied the apparatus and technique of reference [4] to liquid normal deuterium. We analyzed these data in a manner identical to that described for hydrogen. Pressures were converted to bars and temperatures adjusted to IPTS-68 [11]. A fit of the molar volume data, in cm^3/mole, to eqs (4) and (6) gives the following parameter values: $a_1=-21.1311$, $a_2=8.42177\times10^2$, $a_3=-2.72227\times10^2$, $a_4=8.41630\times10^4$, $a_5=-4.21649\times10^6$, $a_6=-0.523114\times10^8$. The standard and average absolute deviations of the molar volume measurements from the calculated equation are 0.032 and 0.085 cm^3/mole, respectively.

[13] Driessen, A.; J. A. de Waal and I. F. Silvera, J. Low Temp. Phys. **34**, 255 (1979).